Geochemistry, Geophysics, Geosystems®

AGU ADVANCING EARTH AND SPACE SCIENCES

RESEARCH ARTICLE
10.1029/2023GC011380

Special Collection:
Through the Arctic Lens: Progress in Understanding the Arctic Ocean, Margins and Landmasses

Prolonged Multi-Phase Magmatism Due To Plume-Lithosphere Interaction as Applied to the High Arctic Large Igneous Province

Björn H. Heyn[1], Grace E. Shephard[1,2], and Clinton P. Conrad[1]

[1]Department of Geosciences, Centre for Planetary Habitability, University of Oslo, Oslo, Norway, [2]Research School of Earth Sciences, Australian National University, Acton, ACT, Australia

Key Points:

- Mantle plumes interacting with changes in lithosphere thickness at craton edges can cause prolonged melting with pulses in the same region
- Rejuvenated melting happens underneath previously melt-affected thinned lithosphere several hundred km downstream of the plume stem
- The timing and duration of rejuvenated melting in models correspond to and therefore may explain observations of magmatic pulses from High Arctic Large Igneous Province

Supporting Information:

Supporting Information may be found in the online version of this article.

Correspondence to:

B. H. Heyn,
b.h.heyn@geo.uio.no

Citation:

Heyn, B. H., Shephard, G. E., & Conrad, C. P. (2024). Prolonged multi-phase magmatism due to plume-lithosphere interaction as applied to the High Arctic Large Igneous Province. *Geochemistry, Geophysics, Geosystems*, *25*, e2023GC011380. https://doi.org/10.1029/2023GC011380

Received 27 NOV 2023
Accepted 8 JUN 2024

Author Contributions:

Conceptualization: Björn H. Heyn, Grace E. Shephard, Clinton P. Conrad
Formal analysis: Björn H. Heyn
Funding acquisition: Björn H. Heyn, Grace E. Shephard, Clinton P. Conrad

Abstract The widespread High Arctic Large Igneous Province (HALIP) exhibits prolonged melting over more than 50 Myr, an observation that is difficult to reconcile with the classic view that large igneous provinces (LIPs) originate from melting in plume heads. Hence, the suggested plume-related origin and classification of HALIP as a LIP have been questioned. Here, we use numerical models that include melting and melt migration to investigate a rising plume interacting with lithosphere of variable thickness, that is, a basin-to-craton setting applicable to the Arctic. Models reveal that melt migration introduces significant spatial and temporal variations in melt volumes and pulses of melt production, including protracted melting for at least about 30–40 Myr, because of the dynamic feedback between migrating melt and local lithosphere thinning. For HALIP, plume material deflected from underneath the Greenland craton can re-activate melting zones below the previously plume-influenced Sverdrup Basin after a melt-free period of about 10–15 Myr, even though the plume is already ~500 km away. Hence, actively melting zones do not necessarily represent the location of the deeper plume stem at a given time, especially for secondary pulses. Additional processes such as (minor) plume flux variations or local lithospheric extension may alter the timing and volume of HALIP pulses, but are to first order not required to reproduce the long-lived and multi-pulse magmatism of HALIP. Since melting zones are always plume-fed, we would expect HALIP magmatism to exhibit plume-related trace element signatures throughout time, potentially shifting from mostly tholeiitic toward more alkalic compositions.

Plain Language Summary Typically, the arrival of a large mantle upwelling ("mantle plume") is expected to cause catastrophic large-scale volcanism that lasts a few million years. However, a massive past volcanic event now distributed onshore and offshore across the Arctic (the High Arctic Large Igneous Province —HALIP) defies this definition. This wide-spread magmatism exhibits dates spanning more than 50 Myr, with several pulses of activity. Based on this prolonged magmatism, it has been questioned whether all of it can be attributed to a mantle plume, despite the geochemistry of basalts indicating a plume source. Here, we show that a plume can cause prolonged and multi-pulse magmatism if it interacts with an increase in lithosphere thickness. Once the plume moves below the thicker lithosphere, hot plume material is channeled along the base of the lithosphere toward the adjacent thinner part, where it can reactivate previous melting regions. At this time, the active plume can be about 500 km away from the melting region, hence plume-related melt cannot be used as a proxy for the plume position at the given time. Based on the models, we suggest that the prolonged HALIP magmatism was caused by a plume interacting with the edge of a craton.

1. Introduction

Located at the geographic top of the world, the High Arctic Large Igneous Province (HALIP), also called HALIP, is one of the most enigmatic volcanic provinces on Earth. Broadly speaking, HALIP is attributed to a range of Cretaceous aged (~130–80 Ma) volcanic and magmatic rocks, currently distributed onshore and offshore around the circum-Arctic (e.g., Døssing et al., 2017; Jowitt et al., 2014; Maher, 2001; Tarduno, 1998). HALIP includes flood basalts (both continental and oceanic), plutonic complexes, dykes, sills, and pyroclastic flows. They are dominantly tholeiitic in nature, but with numerous alkaline suites (e.g., Estrada et al., 2016). Roughly from west to east, localities include the Canadian Arctic Islands, northern Greenland, the central Arctic Ocean (Alpha-Mendeleev Ridge), Svalbard, the Barents Shelf, Franz Josef Land, the De Long Islands, and Siberian shelves (Figure 1). The large geographic footprint of both intrusive and extrusive rocks is partly attributed to the mechanism of emplacement (i.e., mantle plume arrival) as well as subsequent dispersal via post-emplacement

Methodology: Björn H. Heyn
Project administration: Grace E. Shephard
Visualization: Björn H. Heyn, Grace E. Shephard
Writing – original draft: Björn H. Heyn, Grace E. Shephard, Clinton P. Conrad

tectonic motions within the Arctic (i.e., opening of the oceanic Eurasia Basin and the Eurekan deformation, e.g. Pease et al., 2014). HALIP is also linked to significant regional oceanographic and climatic environmental changes (e.g., Galloway et al., 2022).

As with many large-igneous provinces (LIPs) worldwide, a mantle plume is considered to be the primary source of HALIP volcanism. This is supported by several lines of evidence including the widespread distribution of HALIP rocks and the large volume of magmatism (both pointing to a large anomaly of elevated mantle temperatures, e.g., Buchan & Ernst, 2018; Coffin & Eldholm, 1994), geochemistry containing a primitive mantle and/or recycled oceanic lithosphere component (pointing to a deep mantle source, e.g. Estrada, 2015, though alternative, shallow signals are discussed below), a pattern of radiating and circumferential dykes (pointing to a subcircular mantle plume head impinging on the lithosphere, e.g., Buchan & Ernst, 2018; Minakov et al., 2018), and major regional sedimentary pathway reorganizations in the Barents Sea (pointing to significant relative uplift to the north, e.g., Midtkandal et al., 2020). The arrival location of the HALIP plume (Figure 1) is often reconstructed offshore, in the region of the Alpha Ridge (e.g., Buchan & Ernst, 2018) or Lomonosov Ridge (Jackson et al., 2010). Unlike many other LIPs, HALIP does not have a clear hotspot track, though it may be linked to later Iceland plume dynamics and a potential trajectory beneath cratonal Greenland (e.g., Forsyth et al., 1986; Lawver & Müller, 1994; Rogozhina et al., 2016).

Documented ages of HALIP magmatism (Figure 2) spread over a temporal range of ca. 50+ Myr, from ∼131 to 78 Ma, with a potential peak phase around 122 Ma. If Kap Washington volcanics of northern Greenland (71–61 Ma Estrada et al., 2010; Tegner et al., 2011; Thorarinsson et al., 2011) are also included, then this time frame increases to over 70 Myr. The protracted and/or multiple pulses of HALIP pose a particular challenge because most traditionally defined LIPs are erupted in a relatively short amount of time (1–5 Myr for >75 % of the volume). Whilst there are other LIPs that seem to have lasted for over ∼20–30 Myr or more (e.g., Ernst & Bleeker, 2010; Jiang et al., 2020, 2023), a duration of 50+ Myr is uncommon, especially for continental LIPs. Furthermore, other such long-lived and multi-pulse LIPs have typically been attributed to changes in tectonic setting, for example, during extension, seafloor spreading and/or a plume interacting with a mid-ocean ridge (as for the case of Kerguelen; Jiang et al., 2020). This scenario mostly applies to oceanic settings, where a plume can cause and/or interact with an active spreading center, together producing extensive and long-lived melting. As detailed below, it is not clear to what extent contemporaneous seafloor spreading and plume-ridge interaction is applicable to HALIP. Whilst it is conceivable that the first HALIP pulse represents a volumetric majority, any time-dependent constraints for HALIP volumes are currently too poorly constrained to determine (see discussion in Section 6). We return to a large-scale and simplified approach and ask: could a mantle plume potentially cause over 50 Myr of intermittent and spatially variable melting without invoking an additional shift in tectonic regime?

One element to this complexity is the geochemical signature of HALIP rocks, which could potentially constrain the origin of the melts. Plume-derived melts are expected to have very different geochemical signatures than melts derived from the depleted asthenosphere. However, there are significant variations in composition between different localities, including those within and between the Canadian and Eurasian sectors, and similar sample ages. Broadly speaking, there seems to be consensus that an upwelling mantle plume was involved (albeit the more ambiguous terms “asthenospheric upwellings” or “decompressional melting” are sometimes referred to). However, the significant geochemical heterogeneity makes it difficult to clearly discriminate between sources and points to one, several, or all, of the following contributions in HALIP magmas: mantle plume material of deep origin that is potentially geochemically heterogenous in nature (e.g., ocean island basalt or recycled oceanic crust signals), crustal contamination, entrainment of sub-continental lithospheric mantle (SCLM), and/or an enriched sub-lithospheric mantle derived from an earlier paleo-Arctic subduction zone and slab (metasomatic signal e.g., Hadlari et al., 2018; Shephard et al., 2016). In summary, most of the analyzed volcanic rocks to-date point to a geochemical signature that can be attributed to a mantle plume, with considerable geochemical variability potentially derived from the local interaction of the magmas with the lithosphere and crust (e.g., Deegan et al., 2023).

Alternatives to a purely mantle plume origin of HALIP magmatism have been proposed. Rift-related magmatism and associated decompression melting, possibly due to the opening of the Amerasia Basin to the north (e.g., Tegner et al., 2011) or even Labrador and Baffin Bay toward the south (e.g., Thorarinsson et al., 2011), have been invoked. The timing of opening (including rifting, seafloor-spreading, and/or hyper-extension) is relevant because rift-related magmatism may have caused or enhanced HALIP magmatism, at least in part. However, the

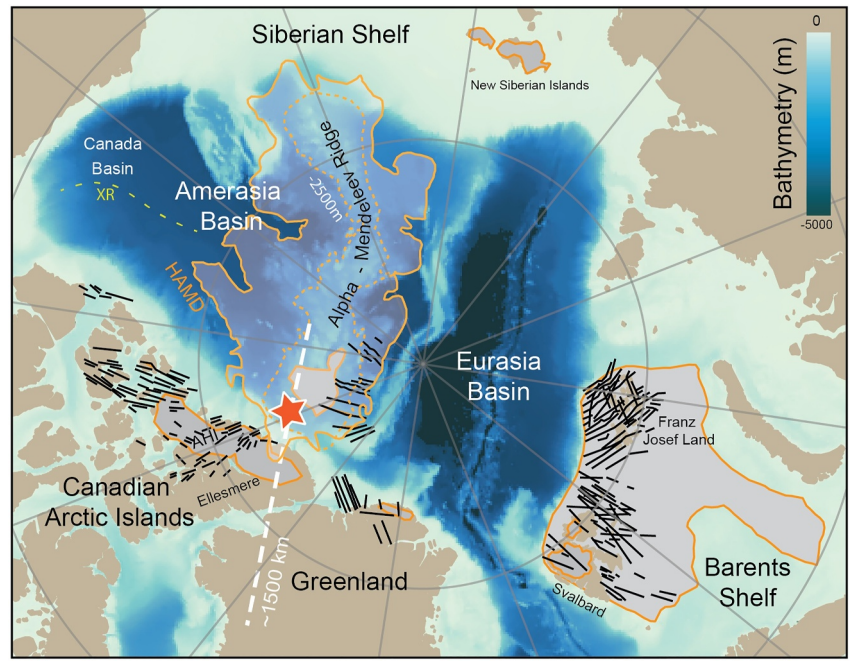

Figure 1. Overview of the Arctic domain at present-day (bathymetry from IBCAO; Jakobsson et al., 2012) with High Arctic Large Igneous Province (HALIP) localities in black lines (mapped or inferred dyke swarms), and orange and gray polygons (proposed HALIP regions beyond those of dykes) as compiled from various sources (Døssing et al., 2017; Jowitt et al., 2014; Minakov et al., 2018; Polteau et al., 2016). HAMD marks the High Arctic Magnetic Domain of Oakey and Saltus (2016) and XR (green dashed line) shows an extinct spreading ridge in the Canada Basin inferred from gravity low (Grantz et al., 1998). The short dashed orange contour is the −2,500 m bathymetry line outlining the Alpha-Mendeleev Ridge; the star is the potential arrival site of the HALIP plume; the long dashed white line approximately marks the ∼1,500 km long NW-SE transect traversing from the Amerasia Basin to Sverdrup Basin to the Greenland Craton as used in the numerical models (basin-margin-craton). AHI is Axel Heiberg Island. Note: at the initial HALIP pulse at around 122 Ma (Figure 2), the tectonic configuration was different—the Amerasia Basin had likely recently opened, the Eurasia Basin did not exist, and Eurekan deformation had not yet occurred.

kinematics and timings of Amerasia Basin opening, or sub-regions thereof (e.g., Canada Basin, Alpha-Mendeleev Ridge, Makarov and Podvodnikov basins), have been long discussed in the Arctic community (e.g., Døssing et al., 2017; Grantz et al., 2011; Shephard et al., 2013), with numerous geological and geophysical data sets invoked and geodynamic models proposed. When considering regional rifting, ages as early as the middle and Late Jurassic have been proposed, but many focus on an Early Hauterivian (∼132 Ma) breakup unconformity (e.g., Embry, 1991; Grantz et al., 1998, 2011). For constraining seafloor-spreading, interpretations of magnetic lineations are particularly valuable but generally require opening to have largely occurred before (or after) the Late Cretaceous Normal Superchron (CNS; ∼121–83 Ma, Cande & Kent, 1995). Studies looking at remnant magnetic anomalies in the Canada Basin have suggested that oceanic-style opening likely occurred somewhere within ∼140–120 Ma, depending on timescales and spreading rates applied (e.g., Døssing et al., 2020; Zhang et al., 2019).

Somewhat conversely, it has also been suggested that the arrival of the HALIP mantle plume caused the opening of the Amerasia Basin (e.g., Mukasa et al., 2020) and, for example, that the elongated shape and intruded nature of the Alpha-Mendeleev Ridge reflects contemporaneous plume-ridge interaction. While a detailed synthesis of Amerasia Basin-centered observations and models is beyond the scope of this paper, the existing data imply that Amerasia Basin opening occurred largely before, or was partly contemporaneous with, the first main pulse of HALIP (which occurred around 122 Ma, Figure 2; Dockman et al., 2018). In such a scenario, rifting/opening may have affected the first HALIP pulse, including by providing additional volumes of melt, but rifting does not explain secondary or later pulses. For the younger HALIP pulses, especially those in the Canadian Arctic post ∼120 Ma, (i.e., second and third pulses at about 95 and 81 Ma, Figure 2) Dockman et al. (2018) questioned the need for a plume for the younger phases of HALIP, calling upon multi-phase (decompression) melting and thermal erosion caused by edge-driven convection related to the inherited lithospheric structure of region.

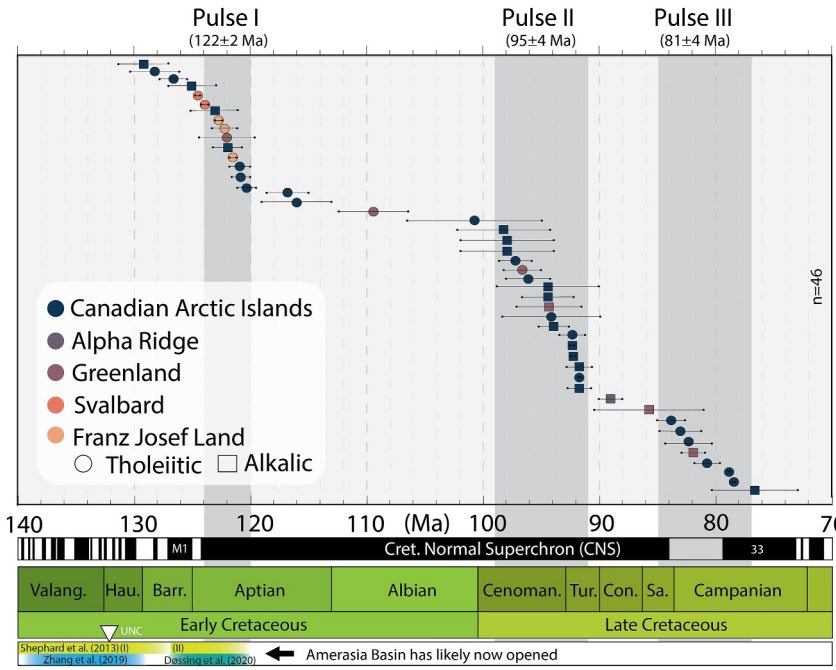

Figure 2. Summary of main High Arctic Large Igneous Province dates and the three proposed pulses, colored by general Arctic location and divided into tholeiitic (circle) and alkaline (square) samples with 2 sigma error. Redrawn from the compilation of Dockman et al. (2018), which was in turn based on several U-Pb and $^{40}Ar/^{39}Ar$ studies from Corfu et al. (2013), Estrada (2015), Estrada and Henjes-Kunst (2004), Evenchick et al. (2015), Jokat et al. (2013), Kontak et al. (2001), Villeneuve and Williamson (2006), and supplemented with four dates from Deegan et al. (2023). Bottom-most bar details selected timings proposed for the opening of the Canada/Amerasia Basin including Shephard et al. (2013) for (I) the Canada Basin and (II) wider Amerasia Basin, and recent magnetic anomaly based interpretations of Zhang et al. (2019) and Døssing et al. (2020), and references therein for timescales. UNC refers to the Early Hauterivian unconformity.

However, general modeling studies such as by Manjón-Cabeza Córdoba and Ballmer (2021, 2022) and Negredo et al. (2022) show that, at least for oceanic lithosphere, edge-driven convection alone rarely produces and sustains magmatism, and any related volumes of magma are small. Thicker continental lithosphere could further reduce any melting resulting from edge-driven convection, whilst on the other hand a more fertile composition may facilitate melting. In any case, it is worth noting, and is discussed later within our paper, that edge-driven convection and a plume might not be mutually exclusive (Manjón-Cabeza Córdoba & Ballmer, 2021, 2022), including for the case of HALIP.

Thus whether HALIP rocks and their origins should be sub-divided temporally, geographically and/or by a causal mechanism remains an active question discussed within the Arctic geoscience community. In this study we consider a simple, first-order scenario by returning to a plume hypothesis, and testing whether a mantle plume arrival and related time-dependent flow can drive HALIP magmatism as a whole. A key question is therefore under which circumstances can plume-lithosphere interactions explain the long-lived volcanism and pulses observed for HALIP? Is an additional process such as rifting or a major pulse in plume flux required, or is there an explanation that does not invoke additional external dynamic events? A regionally focused study of HALIP is therefore pertinent, and focusing on the HALIP localities in the Canadian Arctic Island offers an opportunity to evaluate the spatial and temporal characteristics of melting. Furthermore, melting and melt migration have not yet been incorporated into numerical models of plume-lithosphere interaction. Here we develop such models, and apply them to the High Arctic LIP. We suggest that a plume interacting with pre-existing lithosphere-asthenosphere boundary (LAB) topography across the Arctic can produce prolonged and pulsating magmatism across a large area, while other mechanisms may play a secondary role in the emplacement of HALIP.

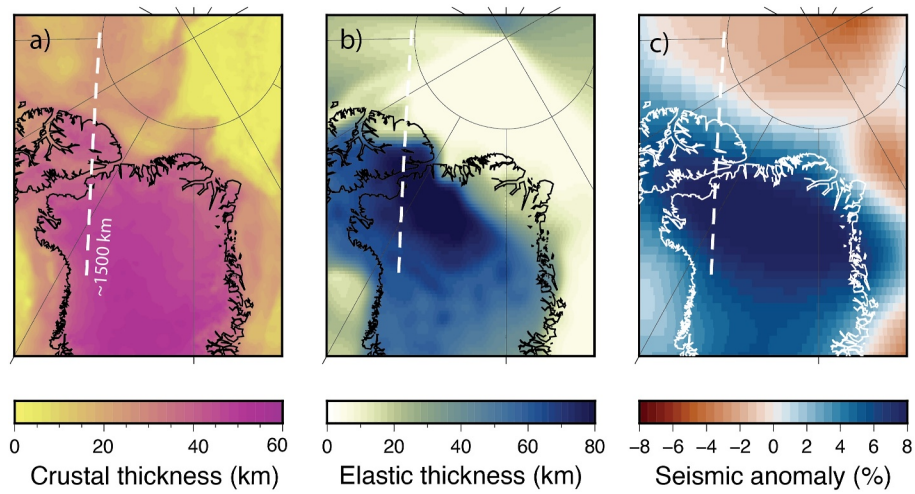

Figure 3. Geophysical data sets for the Canadian Arctic Island and Greenland region overlain with representative location of the model 1,500 km transect from Figure 1 (white dashed line). (a) Crustal thickness from ArcCRUST (Lebedeva-Ivanova et al., 2019), (b) elastic thickness from Steffen et al. (2018), and (c) *P*-wave seismic velocity anomaly at 150 km depth from SL2013sv (Schaeffer & Lebedev, 2013).

2. Constraints on the Timing and Geochemistry of HALIP Magmatism From the Sverdrup Basin

The Sverdrup Basin is a ca. 1,000 km along-strike Carboniferous to Paleogene rift basin, located at the northern edge of the North American continent. It encompasses Ellesmere, Axel Heiberg and Melville islands, amongst others (collectively the Canadian Arctic Islands). These islands are host to several HALIP localities (Figure 1). At present-day, the basin includes changes in crustal (Figure 3a) and lithospheric thickness (Figure 3b) from north to south that reflect its long-lived tectonic history, and such heterogeneity likely existed in past times as well (e.g., Ellesmerian orogeny). While the numerical models we present do not include geochemical complexities, we find it is nonetheless important to consider the geochemical and geochronologic heterogeneity here in the context of underlying melt-inducing processes and tectono-magmatic origins, which together comprise the definition of HALIP.

Numerous field campaigns (including those in Figure 2) reveal varied geochemical and isotopic signals from HALIP. The arrival of a mantle plume is typically associated with (continental or oceanic) flood basalts and tholeiitic suites, with alkaline magmatism frequently pre-, syn-, or post-dating this (e.g., Coffin & Eldholm, 1994). Alkaline magmatism in continental settings may form distally to the main zone of extension (or the mantle plume) and can often be used to test whether the same mantle is sampled between tholeiitic and alkaline suites. The later alkaline suites of HALIP in the Canadian sector appear to be more low-degree mantle melts (Bédard, Troll, et al., 2021) and/or deeper sourced (Dockman et al., 2018) as compared to their tholeiitic counterparts. The alkaline sites are also regionally confined toward the east (not found in Axel Heiberg Island), with the extrusive alkaline lavas only found in the northern part of Ellesmere Island (e.g., Dockman et al., 2018; Trettin, 1991).

While dating methods vary, Dockman et al. (2018) summarized three pulses of Canadian HALIP magmatism; 124–120, 99–91, and 85–77 Ma. As in other circum-Arctic localities, these HALIP magmas are dominated by tholeiitic-type rocks, such as the Isachsen Formation. These are proposed to have an enriched mantle (EM)-like signature and widespread crustal contamination (e.g., Bédard, Saumur, et al., 2021; Naber et al., 2020). However, there are also least two younger groups of alkaline rocks in the Sverdrup Basin region, which are much smaller in volume. Dockman et al. (2018) describe an overlap period of tholeiitic and alkaline magmatism from ca. 100–85 Ma. As recently detailed in Bédard, Saumur, et al. (2021), Bédard, Troll, et al. (2021), these alkaline suites include the ∼96 Ma Fulmar Suite (including Strand Fjord formation), which are suggested to resemble EM-type ocean island basalts with little crustal contamination and a widespread source (apatite-rich) similar to the dominant tholeiites. That said, however, the Fulmar Suite includes Hassel Formation rocks which exhibit a depleted lower crust signal. Two additional, geochemically similar alkaline suites include the 92–93 Ma Wootton

Intrusive Complex with plutonic rocks and the 83–73 Ma Audhild Bay Suite (also referred to as the Hansen Point volcanics) with mafic alkaline rocks. These younger localities are thought to resemble HIMU ocean island basalts but with some crustally derived signals, including potentially shallow melting due to flat heavy rare earth profiles. Bédard, Troll, et al. (2021) concluded that northern Ellesmere Island magmas are derived from variably sampled heterogeneous regions in the SCLM, and do not rule out a mantle plume source.

This geochemical diversity emphasizes the unique characteristics and challenging nature of disentangling shallow-and-deep HALIP processes and the underlying geodynamic causes of HALIP. Do different geochemical signatures represent a different origin of melts (e.g., Tegner et al., 2011), or do they dominantly reflect shallow (crustal) processes of magma assimilation (e.g., Deegan et al., 2023)? The regional tectonic setting of HALIP, including along the Canadian margin, includes an ocean basin to rifted margin to cratonic margin setting, and has undergone several phases of tectonic events both pre- and post-HALIP emplacement. This tectonic legacy has imparted a significant amount of structural and compositional variation into its crust and lithosphere (Figure 3), which may in turn have been reactivated or sampled during the more complicated processes of magma migration and fractionation, especially during successive melting episodes. While it is beyond the scope of this study to disentangle and understand HALIP geochemistry, we aim to understand if a plume alone could provide the original melts from which HALIP magmatism is sourced.

3. Methods

In order to investigate the dynamics of plume-lithosphere interactions of HALIP, and whether HALIP-style rejuvenated magmatism can occur without major changes in plate configuration or plume flux, we ran 2-D numerical models of mantle convection in Cartesian geometry. We focus on modeling the presence of melt and test the impact of variable lithosphere thickness on melt generation relevant to the emplacement of HALIP, that is, the prolonged nature of magmatism and its pulsations. Modeling is done using the open source finite element code ASPECT v2.4.0 (Bangerth et al., 2022; Dannberg & Heister, 2016; Heister et al., 2017; Kronbichler et al., 2012), which includes melting/freezing and two-phase flow melt migration under Darcy's law (Dannberg & Heister, 2016; Dannberg et al., 2019). Active melt and melt residue are tracked via the compositional fields "porosity" and "peridotite," respectively. For every time step of mantle convection, the motion of the melt is solved assuming that melt of density ρ_m and viscosity η_m moves through the pore space of the solid matrix, which is parameterized by the permeability k that depends on the reference permeability k_0 and the amount of melt present. Hence, melt can move independently from the solid, and advects heat with the flow. Since melting and freezing typically occur on shorter time scales than mantle convection, melt reactions are calculated on sub-timesteps assuming that the melt is in equilibrium with the surrounding material. In our models, reaction time steps are set to a maximum of 100 yr, and at least 20 reaction time steps are calculated per advection time step. A more detailed description of the implementation of the two-phase flow and the melting/freezing reaction calculation can be found in Dannberg and Heister (2016), Dannberg et al. (2019) and references therein. Since we assume porosity-driven flow, our model cannot produce magma chambers, dykes/sills or extrusive volcanic products.

Since we focus on upper mantle dynamics, the effects of compressibility and depth-dependence of parameters except for viscosity are small (Albers & Christensen, 1996), hence we can use the Boussinesq approximation. To capture the proposed arrival location of the HALIP plume, we have chosen an approximately NW-SE transect (present-day coordinates) which traverses the Amerasia Basin, Sverdrup Basin of the Canadian Arctic Islands, cratonic Canadian shield, and the northernmost Greenland craton. Two sets of model domain sizes are run, and were chosen to minimize boundary effects, while keeping domains small enough to limit computational costs, as well as allow for a systematic study of different boundary conditions and plate configurations. In the horizontal direction, models have extents of either 1,500 or 4,000 km, with a vertical dimension of 600 or 800 km, respectively. The larger domains are necessary for models with a moving plate. We use adaptive mesh refinement to resolve melt migration, with resolution within each model varying from about 25 × 25 km in areas of the upper mantle away from the plume, to about 3 × 3 km along the surface, the LAB, the melting areas and within the mantle plume.

Given the uncertainty in relative and absolute Arctic plate tectonic reconstructions during the Cretaceous and plume dynamics, a useful first approximation for HALIP is to model a mantle plume arriving under a stagnant tectonic plate (no-slip conditions). This simulates a scenario in which there is no relative motion between the

plume and the plate, but does not necessarily imply that there was no plate motion at all. On the other hand, during the time of HALIP emplacement, the high Arctic had recently undergone or was actively undergoing relative tectonic motions, as well as an overall northward motion in an absolute reference frame. Analysis of a global plate model for the region (Shephard et al., 2013), suggests plate motion in the order of 2 cm/yr relative to the mantle. This also matches suggestions that the HALIP plume later passed underneath Greenland (e.g., Martos et al., 2018; Steinberger et al., 2019), that is, relative motion between the plate and the plume (with the plume moving relatively to the south). To account for this, we investigate models with two different surface-mantle motion scenarios:

1. Six cases with a stagnant plate: model domain with dimensions of 1,500 × 600 km, up to two steps in lithosphere thickness, zero-slip boundary condition at the surface, and free-slip for all other boundaries
2. Seven cases with imposed plate velocity: model domain with dimensions of 4,000 × 800 km, up to two steps in lithosphere thickness moving over the plume, an imposed plate velocity of 2 cm/yr at the top, imposed plate velocities at the side walls to balance inflow and outflow, and free-slip at the bottom

Building from the models presented by Heyn and Conrad (2022), we keep the temperature along the top and bottom boundary fixed to 273 and 1,623 K, respectively, and the initial temperature is described by a linear gradient within the thermal lithosphere of thickness d (defined by the 1,500 K isotherm), and a linear gradient from the base of the lithosphere to the bottom of the domain. The choice of the initial temperature profile and the solidus are further discussed in Text S1 in Supporting Information S1. Present-day estimates of lithospheric thickness (Figure 3b) and upper mantle structure (Figure 3c), constrained using seismic and gravity data, vary significantly across our transect. Although these regions have been affected by post-HALIP tectonic events (such as Eurekan deformation) variations in lithospheric depth across the region, including across the Sverdrup Basin, are likely to have existed at earlier times too, for example, from long-lived and multiple-phases of regional tectonic deformation such as Ellesmerian deformation and Sverdrup rifting (e.g., Anfinson et al., 2012). To account for this, the lithosphere thickness d within the models at the starting condition varies between at least 50 km in the extended basin north of Greenland and up to 200 km for the Greenland craton, but no active rifting is included. The transition between the basin and the craton is simulated by either a gradual increase or up to two "steps" in the depth of the LAB. Details of the model setup are given in the Supporting information and shown in the next section when the respective model results are discussed.

In order to simulate a thermal mantle plume, a plume seed is added to the temperature field at the free-slip bottom of the domain at the initial model time. The seed consists of a Gaussian-shaped anomaly of excess temperature $T_p = 250$ K following the form $\exp(-z/z_d)\,T_p \cdot \exp\left[-\frac{(x-s)^2}{2w^2}\right]$ with the exponential decay thickness $z_d = 200$ km, the width $w = 500$ km and a lateral shift of $s = 500$ km or $s = 3{,}000$ km for the stagnant and moving plate cases, respectively. The Gaussian shaped anomaly is added both as a boundary condition at the bottom, and to the lowest 50 km of the initial temperature field. Models are run going forward in time for 150 Myr, which is sufficient for the plume to rise, convect and interact with the surrounding mantle and lithosphere, therefore capturing the protracted HALIP melting dynamics. For models without imposed plate velocity, the plume seed is removed after 75 Myr in order to limit plume-lithosphere interaction and potential melting times to a duration relatable to HALIP (see e.g. Figure 2).

Viscosity is known to be a key parameter for mantle convection, and it has been shown to play a major role in plume-lithosphere interaction and the amount of lithosphere thinning associated with the plume (Heyn & Conrad, 2022). Extending the models of Heyn and Conrad (2022), we use the same temperature-dependent Newtonian rheology with a step below the asthenosphere, but extend it to include the effects of melting following Dannberg and Heister (2016):

$$\eta_{\text{eff}} = \frac{\eta_j}{\eta_{\text{ref}}} A \exp\left(\frac{E}{RT}\right) \cdot \exp(\alpha_\phi \phi) \cdot \exp(\alpha_\psi \psi) \tag{1}$$

Parameters in Equation 1 are the prefactor A, the activation energy E, and the gas constant R. T describes temperature, and η_j and η_{ref} give the viscosity prefactor for layer j and the reference viscosity used to implement the viscosity jump underneath the asthenosphere. The exponential terms describe the weakening effect of melt with melt fraction ϕ (i.e., the porosity field) and exponential prefactor α_ϕ, and the strengthening effect of melt

Table 1
Characteristic Parameters Used in the Numerical Simulations That Are Referred to in the Text

Parameter	Symbol	Value (unit)
Gravitational acceleration	g	9.81 (m/s^2)
Reference density	ρ_0	3,300 (kg/m^3)
Surface velocity (moving plate cases)	v	2 (cm/yr)
Reference viscosity	η_{ref}	1×10^{22} (Pa s)
Viscosity prefactor for upper/lower layer	η_j	5×10^{22} / 1×10^{24} (Pa s)
Prefactor melt weakening	α_ϕ	27
Prefactor depletion strengthening	α_ψ	0
Viscosity prefactor	A	8×10^{-12} (1/(Pa s))
Activation energy	E	250 (kJ/mol)
Thermal expansivity	α	$3.5 \times 10^{-}$ (1/K)
Specific heat	C_p	1,250 (J/(kg K))
Surface solidus temperature	$T_{\mathrm{sol},0}$	1,350 (K)
Solidus pressure gradient	ΔT_p	7.8/6.8/9.0/7.8/7.8 $\times 10^{-8}$ (K/Pa)
Solidus depletion change	ΔT_ψ	200 (K)
Melt viscosity	η_m	10 (Pa s)
Reference melt density	$\rho_{m,0}$	3,000 (kg/m^3)
Reference permeability	k_0	$1 \times 10^{-}$ (m^2)

Note. The solidus pressure gradient is given for the different models in the order they are mentioned in the text, that is, "2 steps stagnant plate," "2 steps moving plate," "1 ramp moving plate," "1 step moving plate," and "2 steps symmetric moving plate." To see a full list of parameters, including those remaining at the default value specified in the material model, readers are advised to look at the provided parameters files and material model plugin for ASPECT.

depletion via the fraction of melt residue ψ (i.e., the positive peridotite field) and the corresponding exponential prefactor α_ψ, which is in this case set to 0 (no depletion strengthening). All values for the parameters are listed in Table 1.

Melting and freezing are calculated relative to a linearized dry solidus similar to Schmeling (2006) and following the implementation of Dannberg and Heister (2016). While a linear solidus is not directly comparable to petrological data (e.g., Katz et al., 2003), we expect that the effect of higher order pressure terms is small compared to the uncertainty associated with two-phase flow. The solidus is then defined by the surface solidus and the pressure gradient given in Table 1, as

$$T_{\mathrm{sol}} = T_{\mathrm{sol},0} + \Delta T_p p + \Delta T_\psi \psi \tag{2}$$

via the surface solidus $T_{\mathrm{sol},0}$, the pressure gradient ΔT_p and the depletion change ΔT_ψ, with the pressure p and the depletion (positive peridotite field) ψ. Hence, melt depletion increases melting temperatures. A more detailed discussion of the solidus temperature and its relation to the chosen mantle temperature is given in Text S1, including a temperature-depth profile in Figure S1 in Supporting Information S1.

Having described the relevant governing equations and technical terms above, it is important to establish and clarify some definitions. In the following text, melt refers to the active melt fraction at any given time step as obtained from the porosity field. Melt that cools down and freezes is not included. Based on the average melt fraction per model cell and its area, we can calculate the total "melt area," which is technically not a volume since models are 2-D. To convert this into "volume" estimates, we assume that the model cells are 1 km deep with no variation of melt fraction along this direction, resulting in volumes of "km^3 per km assumed model extent." Note, however, that this approach cannot represent real 3-D melt volumes, and models may over-or underestimate melt volumes based on the chosen parameters. A more detailed discussion of how model parameters and the third dimension affect melt volumes, together with a comparison to the very sparse HALIP data, is given in Section 6. As a consequence of the chosen simplifications, we use calculated cumulative (time-integrated) and peak

instantaneous melt volumes for comparison between different models (as far as the parameters allow), and we focus mostly on the potential existence and timing of rejuvenated melting in the models. Instantaneous melt volumes at any given time can be obtained by integrating the porosity field over the domain, and time-integration results in cumulative melt volumes, which allows us to compare melt volumes of different pulses within each model. Due to convergence problems of models with more than 40%–50% melt fractions, we slightly adjust the pressure gradient for models with thicker or thinner lithosphere. A positive side effect of this approach is that maximum melt fractions and total melt volumes are better comparable between models, making it easier to identify the types of LAB topography that facilitate rejuvenated melting of HALIP-style. As mentioned, an overarching aim of the modeling is to inspect the first-order melting trends and dynamics, rather than the absolute and HALIP-wide volumes of melting.

Furthermore, these models neither "erupt" the melt onto the surface of the model (e.g., via extrusive volcanism) nor assume any removal of melt. The latter was undertaken in other studies that calculate melt fractions but do not include a two-phase flow (e.g., Ballmer et al., 2011; Bredow et al., 2017; Steinberger et al., 2019)—some differences between models with and without melt migration are discussed in Sections 5 and 6. The reason that most other comparable mantle convection models to-date do not include actual eruptive volcanism, and few include melt migration at all, is that the computational effort needed to bridge the time and length scales of larger scale mantle convection and eruptive modeling is expensive. This study serves therefore as a first-order estimate on the temporal and spatial dynamics of plume-lithosphere interactions in the presence of melt migration. For now, we simply assume that part of the melt will reach the surface and erupt to form HALIP's extrusive magmatism.

4. Results of Plume-Lithosphere Interaction With Melt Migration

The basic plume-lithosphere interaction for melt-free models including their parameter dependence has been discussed in Heyn and Conrad (2022). To summarize this work, it was found that moving from 2-D to 3-D did not change the overall results of lithospheric thinning or heat flow along a plume track. Here, we continue and extend this work by adding more complexity in the form of melt migration and a non-uniform lithosphere thickness to see whether the interaction of lithospheric steps can explain all or part of the multi-pulse melting behavior and complexity of HALIP. For simplicity, we will first analyze a model with a stagnant plate, before considering moving plate scenarios.

4.1. Stagnant Plate With Two Lithospheric Steps

In order to simulate the transition between a continental edge to a more cratonal interior, that is, from the Sverdrup Basin to the cratonic parts of Greenland, we implemented two lithospheric steps 500 km apart from each other, increasing the lithosphere thickness from 100 km in the northwest (Sverdrup Basin) to 200 km underneath the Greenland craton in the southeast (see Figure 4a). For the initial condition, the plume is placed underneath the first step (toward the left of the domain, representing the northwestern part of the transect), such that it interacts with the lithosphere close to the modeled margin of the continent. The existence of melt at a given time step is indicated by the melt fraction in Figure 4c, which is plotted on top of the temperature field. The first melt appears after about 12 Myr of model time (Figure 4b), when the plume head ascends and reaches a depth of about 200 km. However, initial melt fractions are small and focused in the top area of the plume head (indicated by the black pixels Figure 4c). Within the next 1–2 Myr, the plume head reaches the LAB, and tilts to the left/northwest, toward the thinner lithosphere of the Sverdrup Basin, resulting in strongly asymmetric spreading of the plume material. This asymmetry becomes more pronounced over time, with significantly less plume material spreading below the margin (second step, e.g. visible after 21 Myr).

In this model, melting only occurs beneath the left/northwestern part of the domain (Figure 4c), and its distribution varies significantly with time and space (Figures 4b and 4c). Within just 1 Myr (between 12 and 13 Myr), the melt initially generated in the central portion of the plume head (12 Myr) has risen advectively and reached the LAB. This interaction generates significantly more melt by 13 Myr due to the heat advected with the rising melt and a lower solidus temperature of the ambient material. Additionally, at 13 Myr, a second melting area to the left/northwest has formed in another branch of the plume head around 100–200 km away. This is separated from the older central melt region by a downwelling due to local small-scale convection. The downwelling migrates to the left with time, and is also visible at 21 and 27 Myr. By 21 Myr, the total amount of melt has decreased significantly

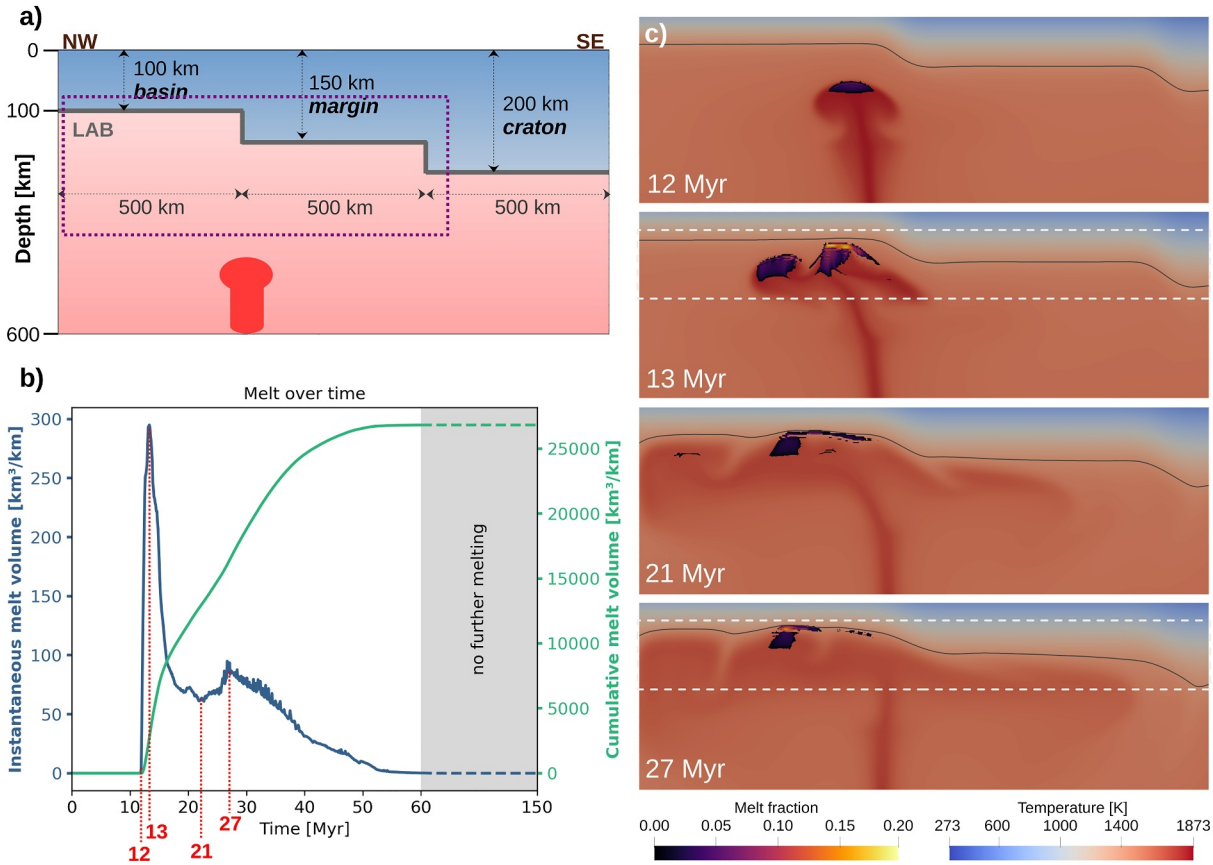

Figure 4. Results for a 2-D model with two lithospheric steps and a stagnant plate, with (a) the model setup including domain dimensions, (b) the instantaneous and cumulative melt volumes over time, and (c) selected snapshots of the temperature field (blue-red colors) overlain with active melt fraction (black-magenta-yellow colors). The 1,400 K isotherm, indicated in (a) and (c) by the dark line, is used as a more stable proxy for lithospheric thickness than the actual lithosphere-asthenosphere boundary (Heyn & Conrad, 2022). The calculated instantaneous melt volumes in (b) correspond to the integrated melt fractions shown in (c) at the indicated times. Note, however, that 2-D models do not give actual melt volumes, but rather 2-D "melt areas" in km^2, which are then for simplicity converted to melt volumes assuming an extent of 1 km in the third dimension (see Section 3 for more information; therefore we use the unit "km^3/km"). The purple dotted rectangle in (a) marks the zoom-in of the domain shown in (c), and the time-evolution of melt volumes in (b) is compressed after 60 Myr since no more melt is generated in the model. White dashed boxes mark the zoom in for Figure 6.

(indicated by lack of purple/yellow colors in Figure 4c and the melt volume in Figure 4b), with the second melting region being almost melt-free, and the initial melting area being spread out and directly interacting with the LAB. Due to the erosion of the lithosphere by melt-induced small-scale convection, the initial melting region experiences rejuvenated strength of melting by about 27 Myr (Figures 2b and 4c, lowermost panel). After this episode of rejuvenated melting, the amount of melt in the model subsides, and the model reaches a melt-free state from about 50 Myr. Even though the mantle plume is still active (switched off at 75 Myr), it does not initiate further melting, neither above the plume nor in any of the previous melting regions. For this model, the duration of melting is ca. 38 Myr (from 12 to 50 Myr).

The setup used here is similar to Negredo et al. (2022), who looked at edge-driven convection and the influence of a mantle plume in the settings of the Canary Islands. Their models show that a plume interacting with a stationary cratonic edge causes a complex and time-dependent flow field within the asthenosphere, with the plume swinging laterally in 2-D models. The resulting melt production is therefore also variable in time and space. While our models do not feature a swinging plume due to the plume hitting directly at the edge of the craton, we also observe a time-dependent melting behavior due to complex local flow patterns. Hence, general dynamics are consistent, although our models with melt migration feature more localized melting zones compared to the models with melt fractions of Negredo et al. (2022).

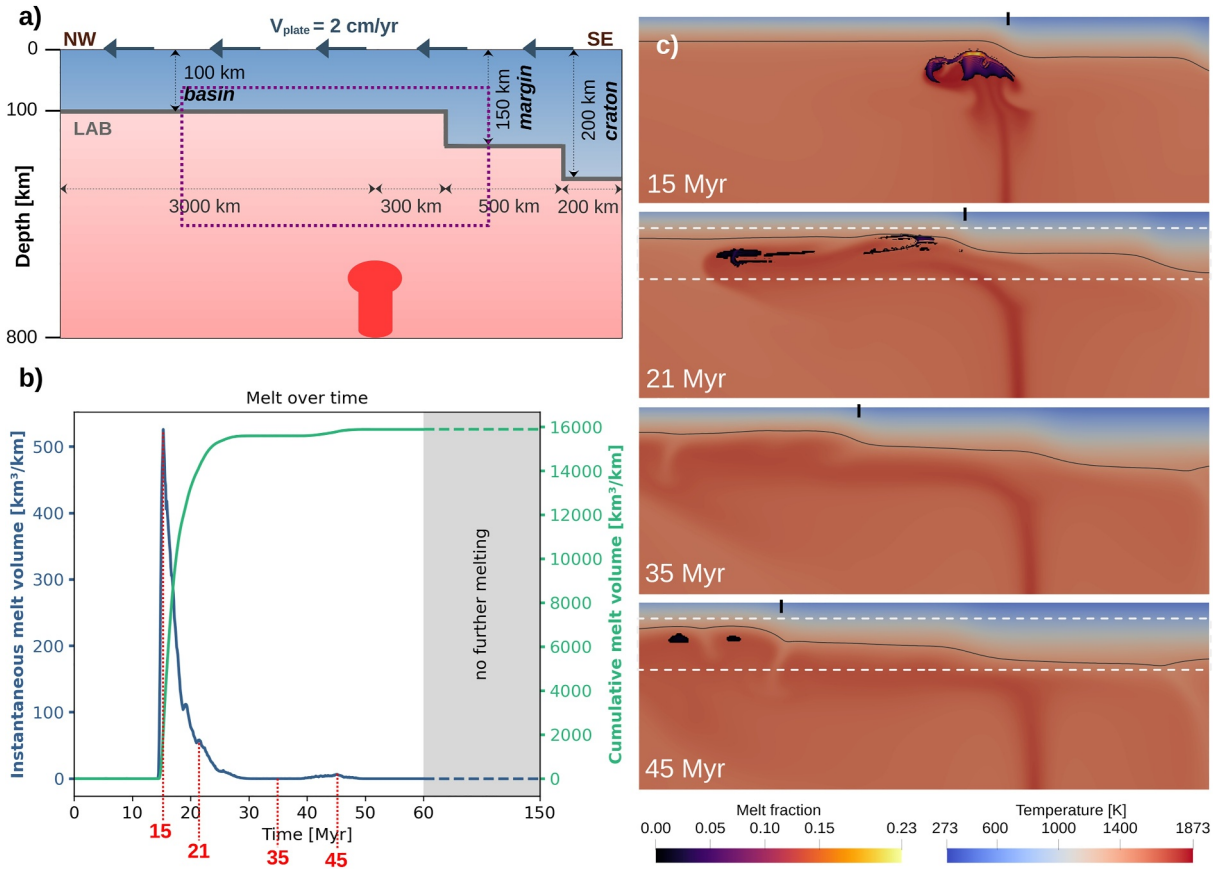

Figure 5. Model setup for a case with two lithospheric steps in which the craton moves over the plume with an imposed plate velocity of 2 cm/yr indicated by arrows (a), instantaneous and cumulative melt volumes versus time (b), and temperature field snapshots with porosity for given times (c). As for Figure 4, the rectangle in (a) marks the area of the temperature snap shots shown in (c), and times from the snap shots in (c) are marked for the instantaneous melt volume in (b). The edge of the basin is marked by the small black vertical line, and the dashed white boxes mark the zoom in used for Figure 6. In contrast to the stagnant plate case, this model reaches a melt-free stage at about 35 Myr, before "rejuvenated" melting occurs at around 42 Myr underneath the right/southeastern corner of the basin.

4.2. Moving Plate With Two Lithospheric Steps

As a next step, we introduce a plate moving with a constant velocity of 2 cm/yr toward the left/northwest, such that the cratonic part of the model eventually moves toward and over the plume. The initial setup is similar to the case shown in Figure 4a, but the model domain is extended toward the north, with the steps starting 300 and 800 km right/southeast of the plume position (see Figure 5a). The distance to the first step is chosen so that the plume head hits the transition between the basin and the continental margin, similar to the stagnant plate case. The first melting occurs at around 14 Myr (Figure 5b), and increases significantly until the plume head hits the LAB at 15 Myr, just in front of the first step where the basin transitions to the margin (Figure 5c). The instantaneous melt volume at the peak of this initial pulse is around 520 km^3/km compared to 300 km^3/km in the stagnant scenario, but the cumulative melt volume is much bigger for the stagnant plate case (about 26,800 km^3/km for stagnant plate vs. 15,900 km^3/km for moving plate). The plume and region of melt at this time, and after, is tilted and deflected toward the left/northwest, toward the thinner lithosphere of the basin. As in the stagnant plate model, the resulting time-dependent melt distribution is spatially inhomogeneous. From ca. 15 to 21 Myr there is a large amount of melting occurring close to the continental margin (first step), and a second melting region is developing about 500 km away from the step to the left/northwest, underneath the basin. With increasing time, the steps move toward the northwest relative to the plume, and at 21 Myr, the continental margin begins to pass over the underlying plume position.

At around 35 Myr, the plume material, as indicated by both the thermal and melt fraction fields, covers an area extending more than 1,000 km away from the active plume, which is now located close to the second step (craton). At this time, there is no more melting occurring in the model. However, over time, the topography of the LAB has

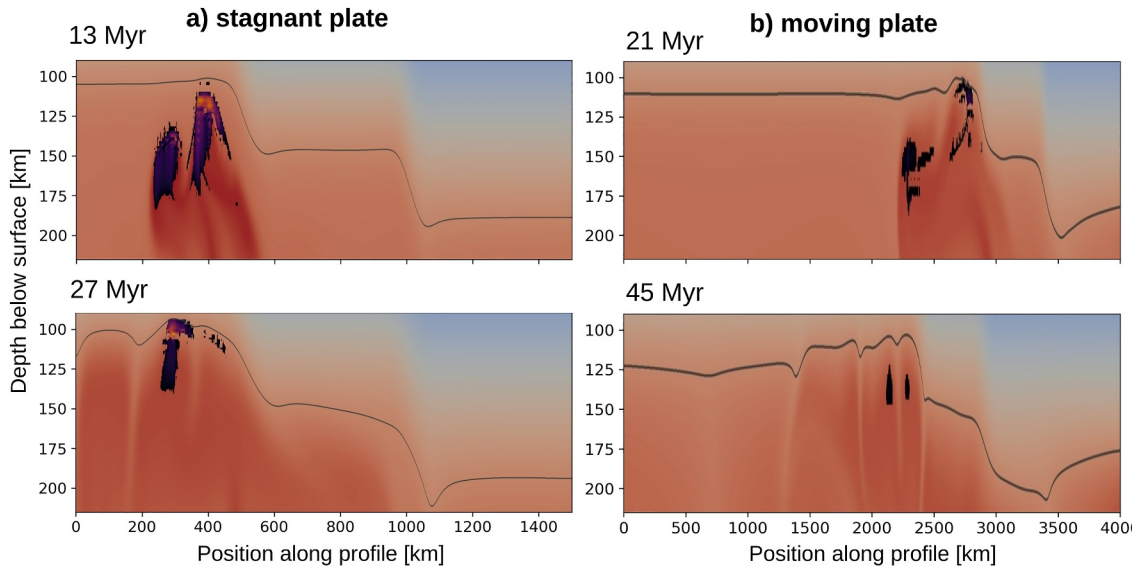

Figure 6. Depth of the 1,400 K isotherm at given times for the models with two lithospheric steps discussed above, with the (vertically stretched) temperature fields and melt fractions from Figures 4c and 5c added. While the arrival of melt at the lithosphere-asthenosphere boundary at 13 Myr in (a) only causes a small reduction in thickness, this effect is significantly more pronounced at later times. Small-scale undulations are related to the presence of melt, and are therefore absent underneath the thicker parts of the lithosphere where no melting occurs.

facilitated the channeling of the shallowest plume material to the left/northwest, toward the thinner lithosphere of the basin. A result of this is that around 45 Myr, plume material arriving at the southeastern edge of the basin in front of the first step is hot enough to melt, causing "rejuvenated" melting underneath the same region of the basin that has previously been affected by melting when the plume head arrived at 15 Myr. This melting occurs in two small pockets, separated by a small downwelling, and is related to local small-scale dynamics of plume material interacting with locally thinned lithosphere and edge-driven convection. Note, however, that the melt fractions and the amount of melt are much smaller than for the first batch of melting (about 0.013 maximum melt fraction and 300 km^3/km cumulative volume compared to 0.23 maximum melt fraction and 15,600 km^3/km cumulative melt volume, respectively). It is also worth noting that this "rejuvenated" melting in this model (cf. the second pulse at 27 Myr in the stagnant case) lasts for at most 10 Myr and happens approximately 20–30 Myr after the initial melting (see Figure 5b). As will be discussed later in more detail, both the length, timing and position of rejuvenated volcanism correspond to the constraints from HALIP data for the first and second pulse of magmatism obtained from Dockman et al. (2018, see also Figure 2), while relative volumes for HALIP are extremely difficult to quantify and may not be represented correctly in the models. Finally, it is noteworthy that the melting at this time occurs more than 500 km away from the active plume stem, indicating that the presence of melt cannot necessarily be used as a constraint for the central plume position at the given time. The duration of melting in this scenario is ca. 21 Myr (from 14 to 35 Myr) or ca. 33 Myr (14–47 Myr) if considering the later, distal episode.

4.3. Lithosphere Thinning and Its Relation to Melting Regions

As described in Heyn and Conrad (2022) for melt-free models (i.e., neither simplified melt fractions nor migration included), the lithosphere above a mantle plume starts to thin as soon as the plume head reaches the LAB due to thermo-mechanical erosion from the plume. With continued plume-lithosphere interaction, the local thinning becomes more pronounced, reaching a maximum value shortly after the plume is removed (for stagnant plate cases) or the respective plume-affected area of the lithosphere has moved significantly (about 200–300 km) relative to the plume (for moving plate cases). In contrast to the melt-free models of Heyn and Conrad (2022), we find that melt rising from the melting zones in the plume head can further reduce lithosphere thickness locally. Figure 6 plots the amount of lithospheric thinning occurring across the horizontal direction at two selected time steps for the two models with two lithospheric steps as discussed above (cf. Figures 4a and 5a). These particular time steps were chosen because they correspond to changes in the melt fraction (e.g., panel b Figures 4 and 5). As seen in Figure 6a for the stagnant plate model (corresponding to Figure 4), thinning starts at 13 Myr above the

melting region (rightmost corner of the basin, next to the first step), but the effects are small since the melt has just reached the LAB. In our models, the presence of melt, and its ability to rise faster than the rest of the plume, reduces local viscosity, increases local dynamics and therefore causes local erosion while a plume with simplified melt fractions at the same point is starting to spread out at about 50 km below the LAB (compare Section 5, Figure 9a). At 27 Myr, the lithosphere is thinnest above the leftmost part of the prolonged primary melting region, where melting is still active (cf. Figure 4c), while the lithosphere thickness is less affected above the second melting region further left/northwest and the area closer to the step where only a small amount of melt remains.

A similar observation can be made in Figure 6b for the moving plate case (corresponding to Figure 5). At 21 Myr, melting is still active in the primary melting zone close to the step, where the lithosphere is significantly thinner than it is further away from the plume. The melting region further to the left/northwest (which did not reach the LAB in Figure 5c at 21 Myr) seems to have little effect on lithosphere thickness at this particular time step. After melting ceases, the lithosphere starts to heal and increases in thickness, as expected. Yet, some of the melt-induced undulations of the LAB remain, and local dynamics can reactivate these areas at 45 Myr. Even though melting itself happens at about 125–150 km depth, the presence of a thinned lithosphere enables local convection that brings plume material up into the melting zone. Note, however, that the local thinning of the thermal lithosphere by melt is limited both in space and time, and reflects the amount of melt that was locally present. As a consequence, the lithosphere beneath the thicker continental margin or the craton to the right of the plume is significantly less affected than the lithosphere beneath the basin, and LAB undulations exhibit much longer wavelengths and lifetimes. Since surface heat flux is a time-delayed and long-wavelength filtered image of the lithosphere thinning (Heyn & Conrad, 2022), it does not reflect the deeper, local, time-dependent melt distributions as predicted in these models. However, if melt were to migrate significantly closer to the surface in these models, then it would exert a larger (but still local) effect on surface heat flux.

4.4. Influence of Lithospheric Structural Variations

In order to investigate the robustness of the rejuvenated volcanism for models with a moving plate, we tested four alternative initial LAB topographies; a gradual ramp, a single step, an indentation set-up and a uniform LAB depth. For the first alternative model, we followed the conceptual model of Dockman et al. (2018), and included a gradual increase of lithosphere thickness from 50 km underneath the Sverdrup Basin to 100 km underneath the Greenland Craton (see Figure 7a), starting initially 300 km right/southeast of the plume. Due to the reduced lithosphere thickness, we increased the pressure gradient for the solidus to reduce overall melt volumes (see Table 1), while all other parameters are kept constant. As for the case of 2 discrete lithospheric steps (Figures 4 and 5), the initial melting zone in the plume head quickly separates into separate regions (here three), separated by local downwellings (15 Myr, Figure 7c). The peak of instantaneous melt volume is the highest for any model, reaching about 700 km^3/km at ca. 15 Myr, and the cumulative melt volume of about 28,600 km^3/km is also the largest of all models. In contrast to the previous case, the plume head is initially less tilted, and one branch of the plume head with melting forms underneath the lithospheric ramp, resulting in a total of three distinct melting zones. Hence, the larger peak of instantaneous melt volume (also reflected in the largest melt fraction of 0.31) and larger cumulative melt volume may partly be related to reduced overall lithosphere thickness, despite the increased pressure gradient of the solidus, and partly to the flatter LAB topography that allows for a third melting zone (instead of two as in the previous cases). At 21 Myr, the two side branches of melting are stretched significantly and have a larger distance from the central melting zone, while showing only marginal amounts of melt (as indicated by only black pixels). The central melting zone at the base of the ramp (right/southeastern edge of the basin) is no longer above the plume, but still maintains a melt fraction of about 0.15, and instantaneous melt volumes reach a small secondary peak (see Figure 7b). However, with the plate moving further to the left/northwest, melting stops completely and the model becomes melt-free (30 Myr), before the central melting region becomes re-activated around 42 Myr. As before, this rejuvenated melting happens about 25 Myr after the initial melting, with much smaller melt volumes (~250 km^3/km cumulative melt volume) and fractions (~0.014) forming over a duration of a few Myr (Figure 7b) and about 600 km away from the plume stem. Hence, multiple melting events can be produced with different initial LAB topographies, as long as the LAB channels plume material toward a thinned area, for example, a region that has been influenced by melt before.

Results from two additional model setup scenarios (a single step or two steps symmetric around a thinned area, Figure 8) show peak instantaneous melt volumes that are smaller than for the cases discussed above. In these cases, there is not a clear sign of rejuvenated volcanism. Note, however, that for both of these cases the plume

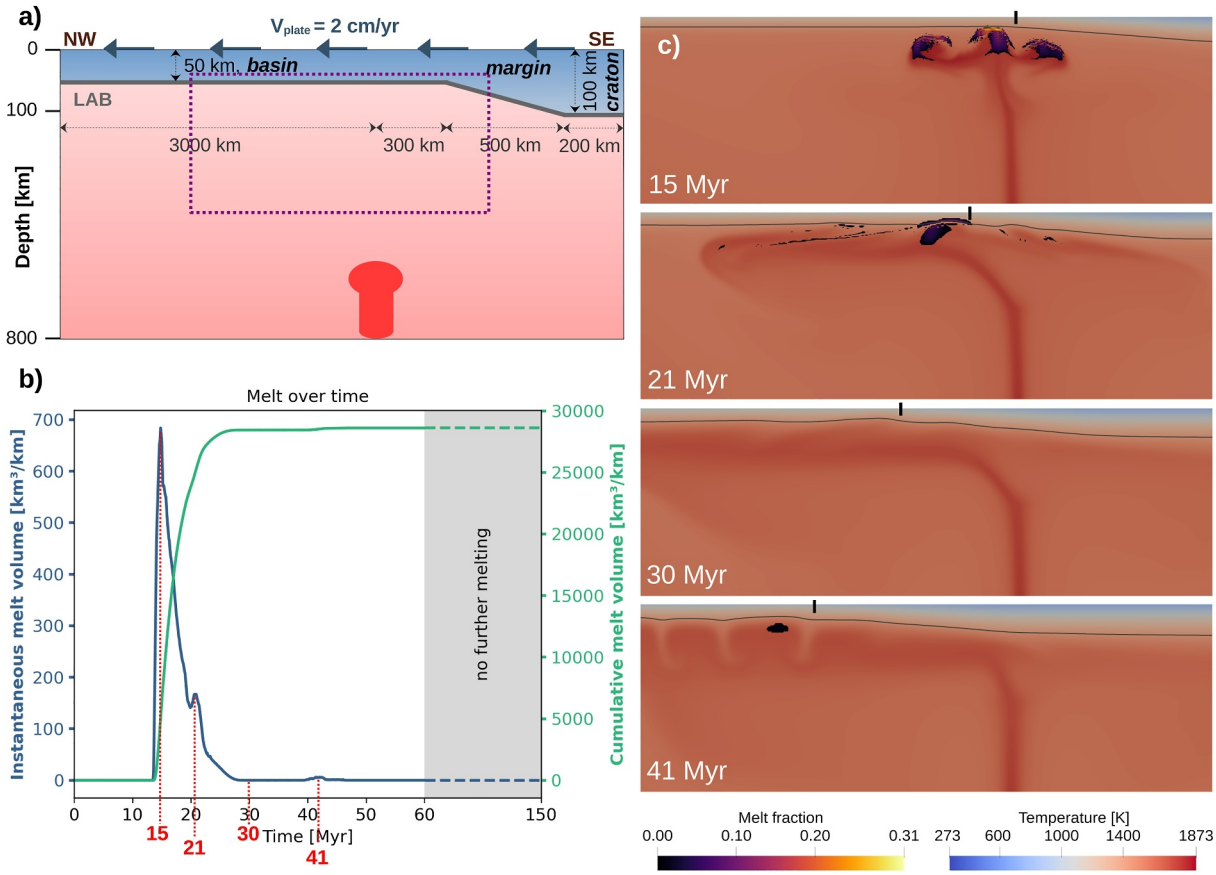

Figure 7. Analogous to Figure 5, but for a model with a gradual transition between the basin and the craton instead of two steps, with the edge of the margin marked by a black vertical line. As before, the imposed velocity is 2 cm/yr, as indicated by the arrows in the model setup (a), and the time evolution of melt volumes is focused on the first 60 Myr (b). As shown in the snap shots of the temperature field (c), the initial melting zone is split into three separate branches at 15 Myr, but only the central branch can sustain substantial melting at 21 Myr. At 30 Myr, the model is melt-free, but experiences rejuvenated melting around 41 Myr underneath the right/southeastern part of the basin.

stays longer beneath the basin and the pressure gradient of the solidus temperature is increased compared to the case with two consecutive steps (see Table 1; the value used is the same as for the stagnant plate case) in order for these models to run without generating >50 % melt fraction, which would make the model numerically unstable. For the single step case (Figure 8b; red line), the lithospheric step to the craton is 500 km away from the arriving plume head, and the extended basin allows the plume material to spread more evenly and easily toward both sides, resulting in an instantaneous melt volume above the plume of about 310 km^3/km at 16 Myr. Due to the smaller initial melt volume, the lithosphere is less thinned, and it becomes more difficult to re-activate any melting zone once the plume interacts with the step (craton). In addition, the lithosphere has more time to heal before the plume material is channeled to the left/northwest by the craton. For the model with a gap (two symmetric steps), it may be expected that plume material rising into the gap of continental lithosphere will be trapped there. In this case, prolonged melting periods may be expected, and perhaps also rejuvenated magmatism once the plume moves underneath the continental lithosphere on the other side of the gap. However, our model (Figure 8b; black line) does not show this, potentially because the initial melt volume in the plume head is too small (~240 km^3/km at 19 Myr) to cause enough lithosphere thinning for rejuvenated melting.

Finally, we compare the results of our cases with variable LAB depth to a case with a moving plate and a constant lithospheric thickness of 100 km, that is, a model without any cratonic or continental parts interacting with the plume ("uniform LAB" in Figure 8a). The pressure gradient of the solidus for this case is set to 7.6×10^{-8} K/Pa, and instantaneous melt volumes for this model are shown in Figure 8a as the dashed blue line. No second pulse of melting occurs, despite the fact that the instantaneous melt volume associated with the arrival of the plume head (~950 km^3/km) is even larger than for the two lithospheric steps or the gradient case, and an overall duration of

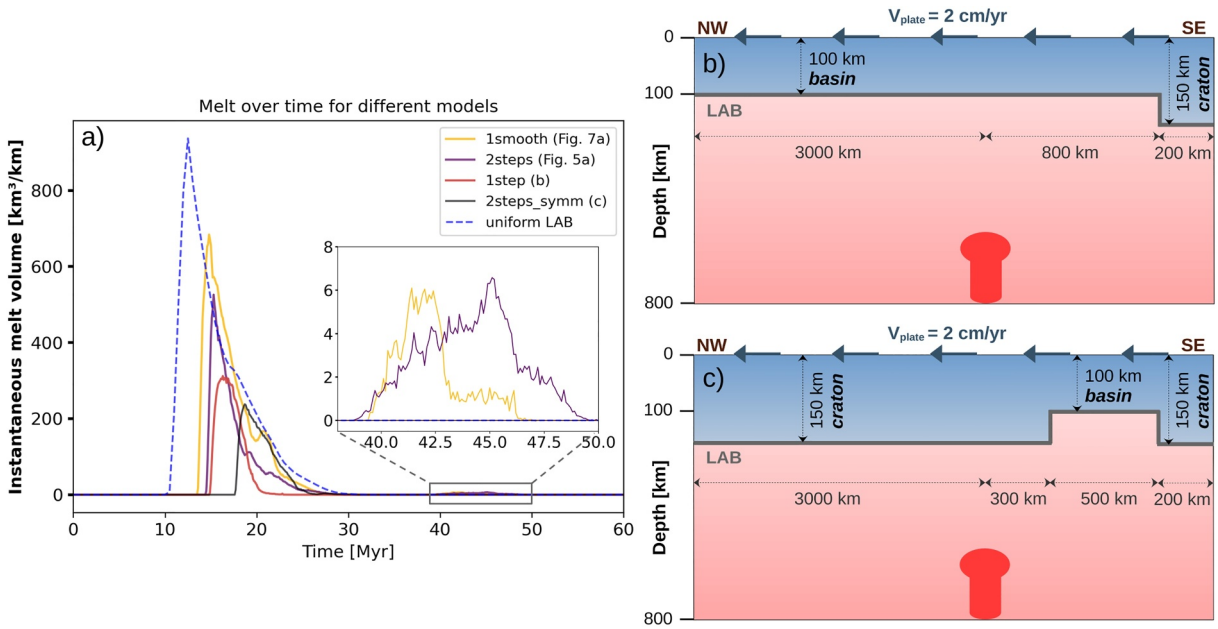

Figure 8. Comparison of instantaneous melt fractions for different initial lithosphere-asthenosphere boundary (LAB) topographies with a zoom-in to the rejuvenated magmatism (a), and the model setups for a case with one step (b), and two symmetric steps (c). Note that the rejuvenated magmatism is only visible for the two lithospheric steps (purple line) shown in Figure 5 and the gradual increase in lithosphere thickness (yellow line) from Figure 7. However, peak instantaneous melt volumes are smaller for the model setups with one step (red line) and two symmetric steps (black line), potentially reducing the chance to observe rejuvenated melting. On the other hand, a model with constant lithospheric thickness (dashed blue line) has the largest maximum instantaneous melt volume of all models shown here, but does not show rejuvenated magmatism. Hence, a large instantaneous melt volume alone seems to be insufficient to generate rejuvenated magmatism if LAB topography is absent.

magmatism of 20 Myr. Since there is no thicker part of the lithosphere moving over the plume, less plume material is directed to a previously thinned area of lithosphere, and melting zones will not be reactivated. Hence, both LAB topography and sufficient initial melting seem to be necessary to generate rejuvenated magmatism that we see for HALIP.

5. Comparison of Melt Migration Versus Melt Fractions

As far as we are aware, this study is the first numerical model to be able to reproduce the style of rejuvenated magmatism observed for HALIP, that is, pulses of magmatic activity in the same region spread over >30 Myr, without the need for changes in plume flux or rifting. Previous work looking at plume-lithosphere interactions or the emplacement of LIPs focused either on specific settings (e.g., Ballmer et al., 2011; Bredow et al., 2017; Manjón-Cabeza Córdoba & Ballmer, 2022; Negredo et al., 2022), or on more general processes (e.g., Duvernay et al., 2022), and used different implementations of melt fractions instead of melt migration. A study closely related to ours is the work of Steinberger et al. (2019), who investigated how the North Atlantic Igneous Province may have been emplaced by the interaction of the Iceland Plume with the Greenland Craton. That study was able to reproduce the reported time frames and melt distributions around Greenland, but did not report on any rejuvenated melting of the type that we see for HALIP. In contrast, the more general work of Duvernay et al. (2022) tested how different settings of lithosphere thickness affect the generation and patterns of melt fractions around cratons. Their results show that melt distribution can vary significantly depending on where the plume impinges on the lithosphere, resulting in a very inhomogeneous distribution of the inferred magmatism over time and space. However, despite the fact that some of the cited studies use more complex melting laws than our models, rejuvenated melting is not commonly observed, and none of the studies show HALIP-style rejuvenated melting. This may be partly due to the lithospheric setting, but the work of Duvernay et al. (2022) does feature lithospheric settings that are similar to our setup, and therefore may have been expected to show rejuvenated melting, but do not. Hence, we suggest that the observation of rejuvenated melting depends not only on the tectonics, but also on the dynamic feedback between melt and mantle flow, which enhances local small-scale convection and lithospheric thinning. Therefore, the characteristics of HALIP may depend both on the tectonic setting and the melt

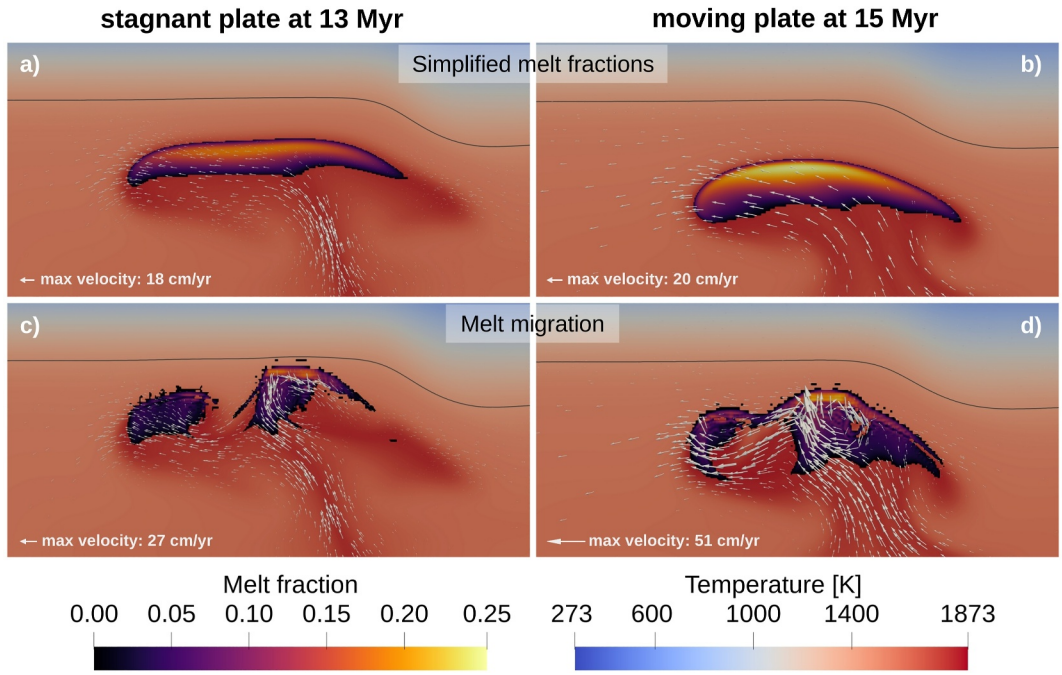

Figure 9. Comparison of 2-D models that implement simplified melt fraction (top row, (a) and (b)) with those that include two-phase flow melt migration (bottom row, (c) and (d)). Models feature two lithospheric steps and either a stagnant plate (left panels (a) and (c), see Figure 4) or a moving plate (right panels (b) and (d), compare Figure 5), and melt is shown on top of the temperature field. Velocities are shown as white arrows, with the scale giving the maximum velocity in each case. While maximum melt fractions are similar in all cases, the melting zones for simplified melt fractions are much broader and more homogeneous than for the cases with melt migration. Note also that plume-related melt in the melt migration cases (bottom row) can rise to shallower depths (compared to the top row, where melting is confined within the plume head), effectively transporting heat to shallower depths.

dynamics. In particular, the implementation of two-phase flow may be necessary to reproduce HALIP's rejuvenated melting.

In order to test this hypothesis, we compare models with the same tectonic setting, but different approaches for implementing melting: simplified melt fractions calculated as a post-processing step based on the temperature field, with no feedback from melt into the dynamics Figure 9 (top panels), and our models with two-phase flow (Figure 9, bottom panels). We test two cases: one with a stagnant plate (Figures 9a–9c) and one with a moving plate (Figures 9b–9d), both with two lithospheric steps. For both the stationary and moving models that only calculate simplified melt fractions (Figures 9a and 9b), the result is a more homogeneous spread of melting across the plume head. The uppermost edge of the plume head, as indicated by the pattern of the melt fraction field, is more or less parallel to the LAB. Furthermore, the melting zone occupies most of the upper third of the plume head, with the largest melt fractions (yellows) in the upper part of the melting zone. The corresponding mantle flow field shows rising material in the plume stem, which spreads parallel to the lithosphere underneath the basin region, with only a small portion of the plume moving underneath the first lithospheric step to the right/southeast (continental margin). In contrast, melt migration models (lower panels) show two separated or loosely connected melting zones (as described in the above section). Melt generation and distribution are very inhomogeneous, with large melt fractions being much more localized than for the models that exclude melt migration. These local dynamics are driven by density and viscosity variations introduced by melt as it evolves through time. This is also reflected in the velocity field; there is increased flow speed and local upwelling in regions where larger amounts of melt are being generated. For example, for the moving plate scenario, the maximum velocity is 20 cm/yr for the simplified melt fraction case and 51 cm/yr when including melt migration. In turn, these localized upwellings cause adjacent downwellings, splitting the melting zones and resulting in a small convection cell next the lithospheric step. Maximum melt fractions (i.e., reaching up to 0.25) at this particular time step are comparable between models with and without melt migration, but total volumes of melt differ significantly due to the smaller melting zones with melt migration.

Table 2
Overview of High Arctic Large Igneous Province Characteristics and How Well They Are Reproduced by the Models

	Model predictions	HALIP observations	
Pulse spacing (1st to 2nd)	~25–30 Myr	~27 Myr	✔
Melt-free period	10–15 Myr	15–20 Myr	✔
Duration 1st pulse	10–15 My	4–15 Myr	✔
Duration 2nd pulse	8–10 Myr	8–10 Myr	✔
Number of pulses	2	3	✘
Relative volumes (1st vs. 2nd)	100×	0–100×	?

Note. A check mark (✔) represents observations that are reproduced reasonably well with the models; a cross (✘) marks a misfit between predictions and observations; and a question mark (**?**) stands for observations that may be explained by the models, but are not well enough constrained by the available High Arctic Large Igneous Province (HALIP) data.

The presence of local dynamics visible in Figure 9 for models with melt migration makes these models significantly more dynamic and time-dependent than models without melt migration. Since melt affects both density, viscosity and temperature, the equations are coupled in a non-linear way, and these models require more computation time and are more sensitive to the chosen parameters. While the effect of melting on local dynamics is not completely new (see e.g., Ballmer et al., 2011; Dannberg & Heister, 2016), melt migration via two-phase flow has not been widely applied to plume settings. Our models show that when melt migrates across the domain, its excess temperature and effect on further melting can cause a sort of positive feedback, resulting in increasing melt volumes and fractions being generated in a localized area; an effect that cannot be observed when calculating melt fractions without melt migration. As a result of these local dynamics, both lithospheric thinning and magmatism will be more variable in time and space when melt migration is included. However, our models cannot simulate volcanism or dyke emplacement, since this would require even finer spatial and temporal resolution. Yet, including local dynamics and melt migration while modeling plume-lithosphere interaction seems to help to reproduce HALIP-style rejuvenated magmatism for complex scenarios such as the tectonic setting associated with the emplacement of HALIP (compare Figures 1 and 2).

6. Discussion

As mentioned in the introduction, two of the main particularities of HALIP are the apparent extensive timing of emplacement (over 50 Myr) and the documented pulses (e.g., earliest magmatism dating at 131 Ma, and pulses at 122, 95, 81 Ma Dockman et al., 2018; Tegner et al., 2011), which lasted about 4–15, 8–10, and 8–10 Myr, respectively. These observations are in strong contrast to most other LIPs around the world, and have sparked alternative explanations for at least part of the magmatism, for example, edge-driven convection north of the Greenland Craton as the source for the secondary pulses (Dockman et al., 2018). Although edge-driven convection is known to be present at lithospheric steps (e.g., Manjón-Cabeza Córdoba & Ballmer, 2021, and references therein), it has been shown that this is likely a short-lived process, and that the amount of melt being generated by this mechanism is small compared to plume-induced melting (Manjón-Cabeza Córdoba & Ballmer, 2021, 2022). Hence, edge-driven convection alone may only sustain small volcanic features such as seamounts, and seems an unlikely explanation for the pulses we see for HALIP. Another mechanism to generate melt in the presence of lithospheric steps is shear-driven upwelling (Conrad et al., 2010), but as for the edge-driven convection, expected melt volumes are small.

In contrast to general models and previous ideas about HALIP emplacement, our numerical models of a thermal mantle plume interacting with LAB topography can explain several aspects of HALIP reasonably well (see Table 2). Most importantly, our models dynamically produce rejuvenated magmatism with comparable timing and duration as has been observed for the first and second pulses of HALIP, although a third pulse cannot be reproduced by our models. The first and second pulses in our models are about 20–30 Myr apart, as are the observations for HALIP. Moreover, the duration of our pulses are about 10–15 Myr for the first major pulse, and 8–10 Myr for the second pulse. While the second pulse in our models has the same duration as the second and third pulse of HALIP, the first pulse seems to be longer in the models than the observations. Note, however, that our first pulse includes deep melting, which may not be directly reflected in extrusive or intrusive magmatism that

has been sampled by petrological studies. In addition, the first pulse in Figure 1 is more spatially spread out than the other pulses, with a potential duration of about 15 Myr (from 130 to 115 Ma). While an extended suite of model runs with alternative parameter setups is beyond the scope of this study, our results show that a mantle plume-related origin for many of the observed HALIP pulses is possible. Furthermore, HALIP magmatism shows compositions and characteristics of plume influence (e.g., Bédard, Troll, et al., 2021; Buchan & Ernst, 2018; Senger & Galland, 2022; Tegner et al., 2011). That said, depending on the paleo-topography of the LAB, edge-driven convection or shear-driven upwelling (in addition to the convective patterns modeled here) may contribute to local dynamics and overall melt volumes and distributions (e.g., Conrad et al., 2010; Duvernay et al., 2022; Manjón-Cabeza Córdoba & Ballmer, 2022; Negredo et al., 2022).

Previous studies looking at melting in plumes have focused on different aspects of the problem, including melting in thermochemically zoned plumes (e.g., Dannberg & Gassmöller, 2018), melting in the presence of continental or cratonic lithosphere (Duvernay et al., 2022), or melting for specific plumes and tectonics settings (e.g., Ballmer et al., 2011; Bredow et al., 2017; Liu et al., 2021; Manjón-Cabeza Córdoba & Ballmer, 2022; Negredo et al., 2022; Steinberger et al., 2019). Even though the various model setups and levels of complexity are different, all studies of plume dynamics mentioned above have in common that they only consider melt fractions, and do not model melt migration, as we do in this study. Some studies vary parameters related to melting changes such as the density (Ballmer et al., 2011; Bredow et al., 2017; Liu et al., 2021; Manjón-Cabeza Córdoba & Ballmer, 2022; Steinberger et al., 2019), viscosity (Ballmer et al., 2011; Bredow et al., 2017; Liu et al., 2021; Steinberger et al., 2019), or melting temperature (Ballmer et al., 2011; Negredo et al., 2022), and the work of Ballmer et al. (2011) on the Hawaiian Plume shows rejuvenated volcanism next to the plume track due to small-scale convection. While the role of small-scale convection is important in both the work of Ballmer et al. (2011) and this study, the cases are not directly comparable. Hawaii is located far from any continent or craton, and is atop oceanic lithosphere older than ∼70 Myr, which is thought to have developed a washboard pattern of LAB topography before the plume hit the lithosphere (Ballmer et al., 2011). In this scenario, rejuvenated melt is generated by the interaction of spreading plume material with this pre-existing pattern next to the plume track. This is not applicable to the Arctic and HALIP. Furthermore, rejuvenated melting in Hawaii seems to happen within about 10 Myr, while HALIP volcanism is spread out over more than 40 Myr.

All of the studies given above assume that melt is extracted from the model, at least if it is above a certain melt fraction, and thus erupted melt volumes can be estimated for any model time (Ballmer et al., 2011; Bredow et al., 2017; Steinberger et al., 2019). However, since melt in those studies does not move independently, melting areas tend to cover broad areas that are similar to the melting regions we obtain for melt fractions in Figure 9 (top panels). This is despite the fact that some of these studies include more complex melting laws than we do. These broad patterns contrast the localized melting zones that evolve with melt migration (Figure 9 lower panels). Since most of the previous studies look at plumes that impinge on oceanic lithosphere, it seems likely that models predict larger melt fractions in the plume head than for continental settings, and that most of the melt would be quickly extracted from the mantle and erupted. Hence, melt migration may play a role in supplying the melt to the base of the oceanic lithosphere, but the melt-lithosphere interaction is potentially limited in the oceanic environment, and the effect of excluding melt migration might be small. On the other hand, a thicker continental or cratonic lithosphere may have insufficient pre-existing fractures to facilitate dyke formations, especially if the lithosphere is intact and not yet altered by tectonics and/or plume-lithosphere interaction, allowing it to act as a porosity barrier (Aulbach et al., 2017). In this case, the fraction of melt that can be extracted from the system may be reduced, potentially even causing larger amounts of melt to pond beneath the lithosphere for a period of time (e.g., Aulbach et al., 2007, 2017; Sun et al., 2020). As a consequence, melt will have more time to interact with the lithosphere and affect local dynamics while trying to rise via two-phase flow, which should therefore be taken into account when doing numerical models.

In contrast to oceanic domains, continental or cratonic lithosphere may pose a barrier to rising melt, especially if the craton is intact (Aulbach et al., 2017). We have shown that if a significant portion of the melt will remain in the asthenosphere or lower lithosphere, it can be expected that the presence of melt significantly alters the local convection patterns (e.g., Figure 9). This feedback between melt and local dynamics is the cause of the rejuvenated magmatism we see in this study, and may explain the main difference between this work and the study of Duvernay et al. (2022), who report complex melting patterns in the presence of cratonic lithosphere, but do not observe rejuvenated volcanism. Hence, including the dynamics of melt migration can facilitate rejuvenated melting and complex melting patterns, such as rejuvenated melting of HALIP-style.

Even though our models can reproduce some aspects of HALIP, for example, a prolonged melting period and the presence of pulses in magmatism (see overview in Table 2), there are several assumptions and limitations that have to be taken into account. First of all, melt migration in ASPECT is modeled via Darcy's law, assuming that melt moves through the pore space of the ambient mantle or lithosphere. As a consequence, we cannot model melt eruptions, LIP emplacement or dyke intrusions. In fact, most of the melt in the models recrystallizes close to the LAB instead of penetrating far into the lithosphere. Hence, our models may overestimate the impact of melting on lithosphere thinning. Furthermore, the amount of melt generated within the plume head is strongly dependent on parameters such as the surface solidus and the pressure gradient of the solidus. Both parameters affect the onset depth of melting as well as the melting range and the melt fraction generated at a given depth. In the models presented here, melting is simplified and therefore might not represent realistic melt volumes. The ability of melt to rise and weaken the lithosphere further depends on the melt viscosity, density, and the permeability of the host rock. In addition, incorporating the effect of latent heat during melting and freezing would further affect melt volumes and melting duration by the associated removal or release of heat. However, since melting regions in our models are continuously replenished by hot plume material, we would expect that the effect is smaller than for edge-driven convection alone. Finally, we only considered melting of dry peridotite, while the presence of water would potentially facilitate more voluminous melting, or melting at lower temperatures or greater depths. Chemical heterogeneities present within the lithosphere or the plume can further affect melt volumes and melt compositions.

A second important simplification is that our models are 2-D, and therefore cannot capture the full dynamics of 3-D plumes. In 2-D, plumes are "semi-infinite sheets" instead of columnar upwellings, and plume material can only spread laterally in one direction beneath the plate. However, Heyn and Conrad (2022) showed that both 2-D and 3-D models follow the same general trend of lithospheric thinning along the plume track in melt-free cases, with even slightly larger amounts of lithospheric thinning in 3-D cases. As a consequence, melting along the plume track is likely to be stronger in 3-D than in 2-D, although probably with only a limited extent of local melting in areas next to the plume track, as Ballmer et al. (2011) found for oceanic lithosphere models. Steps in lithospheric thickness as presented here will have the additional effect of focusing plume material into the direction of the basin and the area of thinnest lithosphere, namely the old plume track. Based on these results, we would expect that most of the small-scale convection and melting would happen along the plume track, independent of the geometry, and that the overall dynamics should be comparable both in 2-D and 3-D models. Locations and timing of melt generation may differ slightly between 2-D and 3-D simulations due to the effect of small-scale convection, especially for the rejuvenated melting, but regions of strongest thinning along the plume track are most prone to rejuvenated melting. Hence, to explain details in regional melting patterns, a 3-D study would be required, but 2-D is sufficient to understand the underlying mechanism of HALIP-style rejuvenated magmatism. In addition, models with melt migration are computationally expensive, making 3-D models difficult to realize. Yet, 2-D models do not allow us to properly estimate melt volumes, since we have no constraint on the width of the melting zone in the third dimension. To convert our melt volume predictions in km^3/km to actual melt volumes, we would have to multiply them by the actual extent of the melting zones in the third dimension, which is likely more than 1 km. Moreover, melting/freezing and melt migration are simplified in the models, and may over- or underestimate melting compared to reality. For these reasons we do not compare our estimated absolute melt "volumes" to estimates for HALIP. We note that it is currently very difficult to estimate melt volumes from HALIP observations because of the large spatial spread of volcanism with significant observational gaps, as well as difficulties to map intrusive and extrusive magmatism (Senger & Galland, 2022; Tegner et al., 2011).

Although modeled melt volumes cannot be compared to observations directly, it is obvious that the rejuvenated magmatism in our models is significantly smaller and more regionally confined than for the initial melting in the plume head (e.g., Figures 5a and 7b). For HALIP, it is extremely difficult to estimate the distribution and volumes of intrusive and extrusive magmatism, both for the initial phase and subsequent pulses (Figure 2). An areal estimate of 80,000 km^2 was proposed for the late-stage (85–60 Ma, third pulse) alkaline volcanism alone as defined by Tegner et al. (2011). More recently an accumulated magma volume of 100,000 km^3 was proposed by Saumur et al. (2016) for the Sverdrup Basin (the Canadian part of HALIP, not including other localities around the Arctic), without discriminating between the timing of this magmatism. Based on field mapping, Senger and Galland (2022) calculated 0.14–2.5 km^3 of emplaced magma in Svalbard alone, and expanded that to a regional (Barents Shelf and Franz Josef Land) time-accumulated magma volume that implies up to 200,000 km^3 based on geophysical data. These estimates do not include the ca. 1.3×10^6 km^2 areal extent of the Alpha Ridge Magmatic

High (HAMH, Oakey & Saltus, 2016; Figure 1), which would equal about 20×10^6 km^3 magma and therefore far exceed the continental (onshore or continental shelf) estimates listed above. Cumulative melt volumes for HALIP may therefore be in the order of $(20–30) \times 10^6$ km^3, but we lack clear constraints on the volumes of individual pulses. Taking the data of Tegner et al. (2011) for the third pulse, we would estimate that the secondary pulses could be about up to two orders of magnitude smaller than the first, but this depends strongly on the timing of HAMH emplacement and proportion of volcanism/magmatism. Hence, it seems plausible that the rejuvenated volcanism we see in our models can explain at least some of the locally confined alkalic magmatism observed for HALIP, but it is difficult to assess whether our model prediction of secondary pulses being about two orders of magnitude smaller than the initial pulse is realistic or not.

Potential deviations between modeled and observed melt volumes may be partly explained by the difference between 2-D and 3-D geometry, the latter of which would allow for more local patches of melting and more realistic melt volumes. In addition, there are several potential mechanisms that could strengthen rejuvenated melting to produce a larger second pulse or even a third pulse of magmatism in the models. As geological data suggests (Figure 1), the central Arctic may have recently undergone or was undergoing opening at around the time of the first pulse of HALIP (e.g., Tegner et al., 2011), with potential episodes of local rifting at later stages. Such thinning, related to extensional tectonics, could be expected to enhance rejuvenated melting for the pulses. The distance to, respective timings of, and magnitudes of the extension/spreading would likely determine the magnitude of melt generation. Therefore improved constraints on plate reconstructions of the Arctic as well as the nature of the Alpha-Mendeleev Ridge (and the HAMH, Figure 1) are essential to explain the peculiarities of HALIP in more detail than presented here. However, as mentioned in the Introduction, several studies postulate that at least the majority of rifting and seafloor-spreading that lead to the opening of the Amerasia Basin occurred before the Cretaceous Normal Superchron, and was therefore before or was contemporaneous with, the first pulse of HALIP magmatism (e.g., Døssing et al., 2020). Thus, while it is possible that a plume, plume-ridge and/or plume-rift dynamics may have caused the HAMH and the first pulse of melting, this scenario does not sufficiently explain the secondary and later pulses. Our numerical models do not include any rifting, and therefore only require the Amerasia Basin to be present and do not require constraints on when or how an opening could have happened. On the other hand, areas of rejuvenated melting in our models would strongly react to small changes in the plate configuration, and hence even brief local extension (e.g., possibly in the Makarov Basin around the latest Cretaceous to middle Paleocene ~69–57 Ma, e.g., Døssing et al., 2017) could possibly lead to extensive local magmatism.

Another option to generate a more voluminous second pulse of melting could be a temporal variation in plume flux, which has been suggested for the Iceland plume based on V-shaped ridge segments in the North Atlantic (e.g., Ito, 2001; S. Jones et al., 2014; S. M. Jones et al., 2002; Parnell-Turner et al., 2014). It seems unlikely that these plume flux changes would be sufficient to trigger secondary HALIP pulses by themselves, but instead would strengthen rejuvenated melting where it occurs based on the dynamics we present. Dynamically, pulses in plume flux could be related to (potentially slab-driven) dynamics at the core-mantle boundary (e.g., Heyn et al., 2020), interaction with edge-driven convection (e.g., Manjón-Cabeza Córdoba & Ballmer, 2022; Negredo et al., 2022), solitary waves (Ito, 2001), plume tilting and interactions at the transition zone (e.g., Neuharth & Mittelstaedt, 2022), and/or an interaction between the plume and an ancient slab found underneath Greenland at about 1,000–1,600 km depth (Shephard et al., 2016). While strong plume flux pulses, extensive seafloor spreading, or continental rifting can generate melting without the dynamic feedback between melt and lithosphere described in this paper, our models show that a previously melt-influenced region of the lithosphere is more prone to rejuvenated melting, and may even experience HALIP-style rejuvenated melting without any external triggers. As a consequence, small changes in plume flux or local and short-lived rifting or extension can be enough to trigger pulses without invoking large-scale changes in plume dynamics or plate configuration.

It is beyond the scope and capability of our models to predict compositions of generated melts, but our models indicate that large parts of the asthenosphere underneath the Sverdrup Basin region may have been influenced by a plume due to the channeling of plume material from the craton to the basin. As a consequence, we would expect that melting zones are plume-fed, with all of the generated melt having more or less plume-influenced compositions. In fact, rejuvenated magmatism in our models is derived from ambient plume material, and not the remelting of frozen melts from the first pulse. However, the composition of melts is expected to change over time as the plume-lithosphere interaction evolves, and could also be influenced by pre-existing mantle chemistry—whether sub-continental or metasomatic mantle. Initial melts are likely to dominantly have the original

(potentially deep-mantle) signature of the plume, at least before extensive interactions and potential equilibration with the lower lithosphere. At later stages, when more lower lithosphere is likely entrained in the local convection cells where melt is generated, melt compositions could shift toward enrichment in lithospheric and/or crustal signatures, for example, EM signatures. During the evolution of the system, further influences may come from pulses in plume flux, whether derived from the transition zone, lower mantle and/or plume-slab interactions. Finally, melt fractions and melting depths change significantly during the evolution of the system in our models (especially for the models accounting for melt migration). The first phase of melting in the plume head is dominated by deep melts at lower melt fractions (that may never reach the surface), which rapidly changes toward predominantly shallower melting with large melt fractions. Over the next few million years, melt is generated at (locally increasingly) shallower depths, but melt fractions decrease until melting stops altogether. Rejuvenated melting is then characterized by low melt fractions at slightly deeper depths than the late stage of the first pulse. As a consequence, magmas can be expected to shift from mostly tholeiitic around the peak of the first pulse, to more alkalic at later stages of the first peak and in the second and third pulses. This trend seems to be supported by the data for HALIP (Figure 2). Models also indicate that the distribution of tholeiitic and alkalic magmatism may be not only time- but also location-dependent, and both types may be present at the same time, similar to what HALIP magmas suggest (Figure 2). However, in order to have a better constraint on the timing and locations of each magma type, we would need to add additional complexities to the model, for example, run 3-D models and include more complex melting laws that track compositions in more detail. Future models could also address the broader HALIP geographic setting (Figure 1), beyond that of the Canadian Arctic Islands focused on here.

7. Conclusions

HALIP is an unusual LIP, if it can even be considered a LIP in the classic sense, because magmatism lasted for more than 50 Myr, with pulses of volcanic activity at around 122, 95, and 81 Ma. Based on existing age dating, the duration of pulses is about 4–15 Myr for the initial stage, and approximately 8–10 Myr for each rejuvenated stage, with a very few instances of recorded ages in between pulses. So far, no conclusive mechanism has been proposed to explain this behavior that does not invoke major changes in plume dynamics and/or plate reconfigurations. This is because LIPs are typically emplaced continuously within a short time, and edge-driven convection alone seems unlikely to explain the extent, duration and volumes of magmatism in the Arctic, even for secondary pulses (Manjón-Cabeza Córdoba & Ballmer, 2021). In this work, we show that the arrival of a mantle plume can produce both prolonged melting periods and multiple events of melting in the same area with similar timing and duration as observed for HALIP for a plume interacting with existing spatial variations in LAB depth. More specifically, the tectonic history of the Arctic suggests that the majority of HALIP was emplaced in an area of actively or recently extended continental lithosphere, which was in turn surrounded by continental and cratonic lithosphere. Notably, our models do not assume active extension, but only require lateral changes in lithosphere thickness that may have been the result of earlier tectonic motions.

After first arriving at around 130 Ma and causing the first HALIP pulse, the plume (which possibly is the same plume that is under Iceland today) eventually passed from below the Sverdrup Basin to beneath the Greenland Craton during the later stages of HALIP magmatism (i.e., post 100 Ma). Our models show that if the initial plume arrived at the base of the lithosphere near the Sverdrup Basin and subsequently moved beneath the Greenland Craton, most of the initial melting and associated lithosphere thinning of the first pulse would happen beneath the basin, resulting in an LAB with strong local undulations. After the craton moved over the plume stem, plume material became channeled toward the basin, where previously thinned regions may have experienced rejuvenated melting due to a combination of plume influence and small-scale convection (potentially with edge-driven convection as a supporting factor) about 25–30 Myr after the initial melting pulse. Both the timing and duration of our predicted pulses are comparable to the observations for HALIP. This mechanism produces HALIP-style rejuvenated magmatism without requiring additional major changes in plate configurations (e.g., rifting) or plume dynamics (e.g., plume flux pulses, or a secondary plume). Our models support a plume-related origin for most or even all the magmatism associated with HALIP. In addition, our models emphasize the importance of dynamic feedback between migrating melt, implemented for example, via two-phase flow, and the local convection patterns in order to reproduce and understand specific characteristics of HALIP, and maybe even other continental or cratonic LIPs.

Melting depths and melt fractions vary through time in the models, and inferred compositions might therefore be expected to change from more tholeiitic magmas for the first peak toward more alkalic magmas for later stages of

the first peak and for secondary pulses, but our models cannot track such changes in detail. Furthermore, while the simplified 2-D model used in this study can explain both the timing and duration of the second pulse of melting for HALIP, relative or absolute melt volumes cannot be compared to observations due to the lack of constraints from HALIP data, and because of the 2-D nature of our models. We note, however, that volumes of predicted rejuvenated magmatism are significantly smaller in our models than the first pulse of melting, which might not be representative for HALIP, and our models do not reproduce a third pulse. On the other hand, the magnitude of the second pulse of melting, and the presence and size of a potential third pulse, may easily be affected by contemporaneous tectonics (especially local extension or rifting), plume flux pulses generated at the core-mantle boundary, or plume-slab interactions, all of which could easily re-activate or amplify rejuvenated melting in areas that have been thinned by melt previously. Finally, a key result of our models is that active melting does not necessarily happen above the plume. Rather, lateral flow of the plume may re-activate local melting in a previously plume-affected region up to a few hundred km away from the current plume position. Such complexity should be taken into account when using plume-related melting to infer plume positions, and when interpreting patterns of magmatism for HALIP and other LIPS or melting events erupting close to continental or cratonic margins.

Conflict of Interest

The authors declare no conflicts of interest relevant to this study.

Data Availability Statement

Data presented in Figures 1 and 2, together with the ASPECT parameter files, ASPECT material model plugin, model data and postprocessing scripts used to generate and analyze the numerical models presented in this paper, are available via Zenodo (Heyn et al., 2024). ASPECT v2.4.0 (Bangerth et al., 2022) is freely available under the GPL v2.0 or later license, and can be accessed via https://geodynamics.org/resources/aspect or https://aspect.geodynamics.org, or via the github page https://github.com/geodynamics/aspect that includes the current development version of the code.

Acknowledgments

The authors acknowledge support from the Research Council of Norway through its Centers of Excellence funding scheme, Project Numbers 223272 and 332523, through the MAGPIE project, Project Number 288449, and through its Young Research Talent scheme for POLARIS—Evolution of the Arctic in Deep Time, Project Number 326238. Computations were made possible by the Norwegian Research Infrastructure Services (NRIS/sigma2) via allocations NN9283K, NS9029K, and NN10003K. We would like to thank the Computational Infrastructure for Geodynamics (geodynamics.org), which is funded by the National Science Foundation under award EAR-0949446 and EAR-1550901 for supporting the development of ASPECT. We further thank Antonio Manjón-Cabeza Córdoba and one anonymous reviewer for helpful feedback, as well as the Associate Editor for comments and for handling the manuscript.

References

Albers, M., & Christensen, U. R. (1996). The excess temperature of plumes rising from the core-mantle boundary. *Geophysical Research Letters*, *23*(24), 3567–3570. https://doi.org/10.1029/96GL03311

Anfinson, O. A., Leier, A. L., Gaschnig, R., Embry, A. F., & Dewing, K. (2012). U–Pb and Hf isotopic data from Franklinian Basin strata: Insights into the nature of Crockerland and the timing of accretion, Canadian arctic islands. *Canadian Journal of Earth Sciences*, *49*(11), 1316–1328. https://doi.org/10.1139/e2012-067

Aulbach, S., Griffin, W. L., Pearson, N. J., O'Reilly, S. Y., & Doyle, B. J. (2007). Lithosphere formation in the central slave craton (Canada): Plume subcretion or lithosphere accretion? *Contributions to Mineralogy and Petrology*, *154*(4), 409–427. https://doi.org/10.1007/s00410-007-0200-1

Aulbach, S., Massuyeau, M., & Gaillard, F. (2017). Origins of cratonic mantle discontinuities: A view from petrology, geochemistry and thermodynamic models. *Lithos*, *268–271*, 364–382. https://doi.org/10.1016/j.lithos.2016.11.004

Ballmer, M. D., Ito, G., van Hunen, J., & Tackley, P. J. (2011). Spatial and temporal variability in Hawaiian hotspot volcanism induced by small-scale convection. *Nature Geoscience*, *4*(7), 457–460. https://doi.org/10.1038/ngeo1187

Bangerth, W., Dannberg, J., Fraters, M., Gassmoeller, R., Glerum, A., Heister, T., et al. (2022). Aspect v2.4.0. *Zenodo*. https://doi.org/10.5281/zenodo.6903424

Bédard, J. H., Saumur, B. M., Tegner, C., Troll, V. R., Deegan, F. M., Evenchick, C. A., et al. (2021). Geochemical systematics of high arctic large igneous province continental tholeiites from Canada—Evidence for progressive crustal contamination in the plumbing system. *Journal of Petrology*, *62*(9), egab041. https://doi.org/10.1093/petrology/egab041

Bédard, J. H., Troll, V. R., Deegan, F. M., Tegner, C., Saumur, B. M., Evenchick, C. A., et al. (2021). High arctic large igneous province alkaline rocks in Canada: Evidence for multiple mantle components. *Journal of Petrology*, *62*(9), egab042. https://doi.org/10.1093/petrology/egab042

Bredow, E., Steinberger, B., Gassmöller, R., & Dannberg, J. (2017). How plume-ridge interaction shapes the crustal thickness pattern of the réunion hotspot track. *Geochemistry, Geophysics, Geosystems*, *18*(8), 2930–2948. https://doi.org/10.1002/2017GC006875

Buchan, K. L., & Ernst, R. E. (2018). A giant circumferential dyke swarm associated with the high arctic large igneous province (HALIP). *Gondwana Research*, *58*, 39–57. https://doi.org/10.1016/j.gr.2018.02.006

Cande, S. C., & Kent, D. V. (1995). Revised calibration of the geomagnetic polarity timescale for the late cretaceous and cenozoic. *Journal of Geophysical Research*, *100*(B4), 6093–6095. https://doi.org/10.1029/94JB03098

Coffin, M. F., & Eldholm, O. (1994). Large igneous provinces: Crustal structure, dimensions, and external consequences. *Reviews of Geophysics*, *32*(1), 1–36. https://doi.org/10.1029/93RG02508

Conrad, C. P., Wu, B., Smith, E. I., Bianco, T. A., & Tibbetts, A. (2010). Shear-driven upwelling induced by lateral viscosity variations and asthenospheric shear: A mechanism for intraplate volcanism. *Physics of the Earth and Planetary Interiors*, *178*(3), 162–175. https://doi.org/10.1016/j.pepi.2009.10.001

Corfu, F., Polteau, S., Planke, S., Faleide, J. I., Svensen, H., Zayoncheck, A., & Stolbov, N. (2013). U–Pb geochronology of Cretaceous magmatism on Svalbard and Franz Josef Land, Barents Sea large igneous province. *Geological Magazine*, *150*(6), 1127–1135. https://doi.org/10.1017/S0016756813000162

Dannberg, J., & Gassmöller, R. (2018). Chemical trends in ocean islands explained by plume–slab interaction. *Proceedings of the National Academy of Sciences*, *115*(17), 4351–4356. https://doi.org/10.1073/pnas.1714125115

Dannberg, J., Gassmöller, R., Grove, R., & Heister, T. (2019). A new formulation for coupled magma/mantle dynamics. *Geophysical Journal International*, *219*(1), 94–107. https://doi.org/10.1093/gji/ggz190

Dannberg, J., & Heister, T. (2016). Compressible magma/mantle dynamics: 3D, adaptive simulations in ASPECT. *Geophysical Journal International*, *207*(3), 1343–1366. https://doi.org/10.1093/gji/ggw329

Deegan, F. M., Pease, V., Nobre Silva, I. G., Bédard, J. H., & Morris, G. (2023). Age and geochemistry of high arctic large igneous province tholeiitic magmatism in NW Axel Heiberg Island, Canada. *Geochemistry, Geophysics, Geosystems*, *24*(11), e2023GC011083. https://doi.org/10.1029/2023GC011083

Dockman, D., Pearson, D., Heaman, L., Gibson, S., & Sarkar, C. (2018). Timing and origin of magmatism in the Sverdrup Basin, northern Canada—Implications for lithospheric evolution in the high arctic large igneous province (HALIP). *Tectonophysics*, *742–743*, 50–65. https://doi.org/10.1016/j.tecto.2018.05.010

Døssing, A., Gaina, C., & Brozena, J. M. (2017). Building and breaking a large igneous province: An example from the high arctic. *Geophysical Research Letters*, *44*(12), 6011–6019. https://doi.org/10.1002/2016GL072420

Døssing, A., Gaina, C., Jackson, H. R., & Andersen, O. B. (2020). Cretaceous ocean formation in the high arctic. *Earth and Planetary Science Letters*, *551*, 116552. https://doi.org/10.1016/j.epsl.2020.116552

Duvernay, T., Davies, D. R., Mathews, C. R., Gibson, A. H., & Kramer, S. C. (2022). Continental magmatism: The surface manifestation of dynamic interactions between cratonic lithosphere, mantle plumes and edge-driven convection. *Geochemistry, Geophysics, Geosystems*, *23*(7), e2022GC010363. https://doi.org/10.1029/2022GC010363

Embry, A. F. (1991). Mesozoic history of the arctic islands. In *Geology of the Innuitian orogen and arctic platform of Canada and Greenland*. Geological Society of America. https://doi.org/10.1130/DNAG-GNA-E.369

Ernst, R., & Bleeker, W. (2010). Large igneous provinces (lips), giant dyke swarms, and mantle plumes: Significance for breakup events within Canada and adjacent regions from 2.5 ga to the present this article is one of a selection of papers published in this special issue on the theme Lithoprobe—Parameters, processes, and the evolution of a continent. Lithoprobe contribution 1482. Geological survey of Canada contribution 20100072. *Canadian Journal of Earth Sciences*, *47*(5), 695–739. https://doi.org/10.1139/E10-025

Estrada, S. (2015). Geochemical and Sr–Nd isotope variations within cretaceous continental flood-basalt suites of the Canadian high arctic, with a focus on the Hassel formation basalts of northeast Ellesmere island. *International Journal of Earth Sciences*, *104*(8), 1981–2005. https://doi.org/10.1007/s00531-014-1066-x

Estrada, S., Damaske, D., Henjes-Kunst, F., Schreckenberger, B., Oakey, G. N., Piepjohn, K., et al. (2016). Multistage cretaceous magmatism in the northern coastal region of Ellesmere island and its relation to the formation of alpha ridge—Evidence from aeromagnetic, geochemical and geochronological data. *Norwegian Journal of Geology*, *96*(2). https://doi.org/10.17850/njg96-2-03

Estrada, S., & Henjes-Kunst, F. (2004). Volcanism in the canadian high arctic related to the opening of the arctic ocean. *Zeitschrift der Deutschen Geologischen Gesellschaft*, *154*(4), 579–603. https://doi.org/10.1127/zdgg/154/2004/579

Estrada, S., Henjes-Kunst, F., Melcher, F., & Tessensohn, F. (2010). Paleocene alkaline volcanism in the nares strait region: Evidence from volcanic pebbles. *International Journal of Earth Sciences*, *99*(4), 863–890. https://doi.org/10.1007/s00531-009-0432-6

Evenchick, C. A., Davis, W. J., Bédard, J. H., Hayward, N., & Friedman, R. M. (2015). Evidence for protracted high arctic large igneous province magmatism in the central Sverdrup Basin from stratigraphy, geochronology, and paleodepths of saucer-shaped sills. *GSA Bulletin*, *127*(9–10), 1366–1390. https://doi.org/10.1130/B31190.1

Forsyth, D., Morel-A-L'Huissier, P., Asudeh, I., & Green, A. (1986). Alpha ridge and Iceland-products of the same plume? *Journal of Geodynamics*, *6*(1), 197–214. https://doi.org/10.1016/0264-3707(86)90039-6

Galloway, J. M., Fensome, R. A., Swindles, G. T., Hadlari, T., Fath, J., Schröder-Adams, C., et al. (2022). Exploring the role of high arctic large igneous province volcanism on early cretaceous arctic forests. *Cretaceous Research*, *129*, 105022. https://doi.org/10.1016/j.cretres.2021.105022

Grantz, A., Clark, D. L., Phillips, R. L., Srivastava, S. P., Blome, C. D., Gray, L. B., et al. (1998). Phanerozoic stratigraphy of Northwind ridge, magnetic anomalies in the Canada basin, and the geometry and timing of rifting in the Amerasia Basin, arctic ocean. *GSA Bulletin*, *110*(6), 801–820. https://doi.org/10.1130/0016-7606(1998)110⟨0801:PSONRM⟩2.3.CO;2

Grantz, A., Hart, P. E., & Childers, V. A. (2011). Chapter 50 geology and tectonic development of the Amerasia and Canada basins, arctic ocean. *Geological Society, London, Memoirs*, *35*(1), 771–799. https://doi.org/10.1144/M35.50

Hadlari, T., Dewing, K., Matthews, W. A., Alonso-Torres, D., & Midwinter, D. (2018). Early triassic development of a foreland basin in the Canadian high Arctic: Implications for a Pangean Rim of fire. *Tectonophysics*, *736*, 75–84. https://doi.org/10.1016/j.tecto.2018.04.020

Heister, T., Dannberg, J., Gassmöller, R., & Bangerth, W. (2017). High accuracy mantle convection simulation through modern numerical methods. II: Realistic models and problems. *Geophysical Journal International*, *210*(2), 833–851. https://doi.org/10.1093/gji/ggx195

Heyn, B. H., & Conrad, C. P. (2022). On the relation between basal erosion of the lithosphere and surface heat flux for continental plume tracks. *Geophysical Research Letters*, *49*(7), e2022GL098003. https://doi.org/10.1029/2022GL098003

Heyn, B. H., Conrad, C. P., & Trønnes, R. G. (2020). How thermochemical piles can (periodically) generate plumes at their edges. *Journal of Geophysical Research: Solid Earth*, *125*(6), e2019JB018726. https://doi.org/10.1029/2019JB018726

Heyn, B. H., Shephard, G. E., & Conrad, C. P. (2024). Prolonged multi-phase magmatism due to plume-lithosphere interaction as applied to the high arctic large igneous province (version 1) [Dataset]. *Zenodo*. https://doi.org/10.5281/zenodo.11092052

Ito, G. (2001). Reykjanes 'v'-shaped ridges originating from a pulsing and dehydrating mantle plume. *Nature*, *411*(6838), 681–684. https://doi.org/10.1038/35079561

Jackson, H. R., Dahl-Jensen, T., & Working Group, L. (2010). Sedimentary and crustal structure from the Ellesmere island and Greenland continental shelves onto the Lomonosov ridge, arctic ocean. *Geophysical Journal International*, *182*(1), 11–35.

Jakobsson, M., Mayer, L., Coakley, B., Dowdeswell, J. A., Forbes, S., Fridman, B., et al. (2012). The international bathymetric chart of the arctic ocean (IBCAO) version 3.0. *Geophysical Research Letters*, *39*(12), L12609. https://doi.org/10.1029/2012GL052219

Jiang, Q., Jourdan, F., Olierook, H. K., & Merle, R. E. (2023). An appraisal of the ages of Phanerozoic large igneous provinces. *Earth-Science Reviews*, *237*, 104314. https://doi.org/10.1016/j.earscirev.2023.104314

Jiang, Q., Jourdan, F., Olierook, H. K., Merle, R. E., & Whittaker, J. M. (2020). Longest continuously erupting large igneous province driven by plume-ridge interaction. *Geology*, *49*(2), 206–210. https://doi.org/10.1130/G47850.1

Jokat, W., Ickrath, M., & O'Connor, J. (2013). Seismic transect across the Lomonosov and Mendeleev ridges: Constraints on the geological evolution of the Amerasia basin, arctic ocean. *Geophysical Research Letters*, *40*(19), 5047–5051. https://doi.org/10.1002/grl.50975

Jones, S. M., Murton, B., Fitton, J., White, N., Maclennan, J., & Walters, R. (2014). A joint geochemical–geophysical record of time-dependent mantle convection south of Iceland. *Earth and Planetary Science Letters*, *386*, 86–97. https://doi.org/10.1016/j.epsl.2013.09.029

Jones, S. M., White, N., & Maclennan, J. (2002). V-shaped ridges around Iceland: Implications for spatial and temporal patterns of mantle convection. *Geochemistry, Geopysics, Geosystems*, *3*(10), 1059. https://doi.org/10.1029/2002GC000361

Jowitt, S. M., Williamson, M.-C., & Ernst, R. E. (2014). Geochemistry of the 130 to 80 ma Canadian high arctic large igneous province (HALIP) event and implications for Ni-Cu-PGE prospectivity. *Economic Geology*, *109*(2), 281–307. https://doi.org/10.2113/econgeo.109.2.281

Katz, R. F., Spiegelman, M., & Langmuir, C. H. (2003). A new parameterization of hydrous mantle melting. *Geochemistry, Geophysics, Geosystems*, *4*(9), 1073. https://doi.org/10.1029/2002GC000433

Kontak, D. J., Jensen, S. M., Dostal, J., Archibald, D. A., & Kyser, T. K. (2001). Cretaceous mafic dyke swarm, Peary Land, northernmost Greenland: Geochronology and petrology. *The Canadian Mineralogist*, *39*(4), 997–1020. https://doi.org/10.2113/gscanmin.39.4.997

Kronbichler, M., Heister, T., & Bangerth, W. (2012). High accuracy mantle convection simulation through modern numerical methods. *Geophysical Journal International*, *191*(1), 12–29. https://doi.org/10.1111/j.1365-246X.2012.05609.x

Lawver, L. A., & Müller, R. D. (1994). Iceland hotspot track. *Geology*, *22*(4), 311–314. https://doi.org/10.1130/0091-7613(1994)022<0311:IHT>2.3.CO;2

Lebedeva-Ivanova, N., Gaina, C., Minakov, A., & Kashubin, S. (2019). Arccrust: Arctic crustal thickness from 3-D gravity inversion. *Geochemistry, Geophysics, Geosystems*, *20*(7), 3225–3247. https://doi.org/10.1029/2018GC008098

Liu, J., Pearson, D. G., Wang, L. H., Mather, K. A., Kjarsgaard, B. A., Schaeffer, A. J., et al. (2021). Plume-driven recratonization of deep continental lithospheric mantle. *Nature*, *592*(7856), 732–736. https://doi.org/10.1038/s41586-021-03395-5

Maher, H. D., Jr. (2001). Manifestations of the cretaceous high arctic large igneous province in Svalbard. *The Journal of Geology*, *109*(1), 91–104. https://doi.org/10.1086/317960

Manjón-Cabeza Córdoba, A., & Ballmer, M. D. (2021). The role of edge-driven convection in the generation of volcanism—Part 1: A 2D systematic study. *Solid Earth*, *12*(3), 613–632. https://doi.org/10.5194/se-12-613-2021

Manjón-Cabeza Córdoba, A., & Ballmer, M. D. (2022). The role of edge-driven convection in the generation of volcanism—Part 2: Interaction with mantle plumes, applied to the Canary Islands. *Solid Earth*, *13*(10), 1585–1605. https://doi.org/10.5194/se-13-1585-2022

Martos, Y. M., Jordan, T. A., Catalán, M., Jordan, T. M., Bamber, J. L., & Vaughan, D. G. (2018). Geothermal heat flux reveals the Iceland hotspot track underneath Greenland. *Geophysical Research Letters*, *45*(16), 8214–8222. https://doi.org/10.1029/2018GL078289

Midtkandal, I., Faleide, J. I., Faleide, T. S., Serck, C. S., Planke, S., Corseri, R., et al. (2020). Lower cretaceous Barents Sea strata: Epicontinental basin configuration, timing, correlation and depositional dynamics. *Geological Magazine*, *157*(3), 458–476. https://doi.org/10.1017/S0016756819000918

Minakov, A., Yarushina, V., Faleide, J. I., Krupnova, N., Sakoulina, T., Dergunov, N., & Glebovsky, V. (2018). Dyke emplacement and crustal structure within a continental large igneous province, northern Barents Sea. *Geological Society, London, Special Publications*, *460*(1), 371–395. https://doi.org/10.1144/SP460.4

Mukasa, S. B., Andronikov, A., Brumley, K., Mayer, L. A., & Armstrong, A. (2020). Basalts from the Chukchi borderland: $^{40}Ar/^{39}Ar$ ages and geochemistry of submarine intraplate lavas dredged from the western Arctic Ocean. *Journal of Geophysical Research: Solid Earth*, *125*(7), e2019JB017604. https://doi.org/10.1029/2019JB017604

Naber, T., Grasby, S., Cuthbertson, J., Rayner, N., & Tegner, C. (2020). New constraints on the age, geochemistry, and environmental impact of high arctic large igneous province magmatism: Tracing the extension of the alpha ridge onto Ellesmere Island, Canada. *GSA Bulletin*, *133*(7–8), 1695–1711. https://doi.org/10.1130/B35792.1

Negredo, A. M., van Hunen, J., Rodríguez-González, J., & Fullea, J. (2022). On the origin of the Canary Islands: Insights from mantle convection modelling. *Earth and Planetary Science Letters*, *584*, 117506. https://doi.org/10.1016/j.epsl.2022.117506

Neuharth, D., & Mittelstaedt, E. (2022). Temporal variations in plume flux: Characterizing pulsations from tilted plume conduits in a rheologically complex mantle. *Geophysical Journal International*, *233*(1), 338–358. https://doi.org/10.1093/gji/ggac455

Oakey, G., & Saltus, R. (2016). Geophysical analysis of the alpha–Mendeleev ridge complex: Characterization of the high arctic large igneous province. *Tectonophysics*, *691*, 65–84. https://doi.org/10.1016/j.tecto.2016.08.005

Parnell-Turner, R., White, N., Henstock, T., Murton, B., Maclennan, J., & Jones, S. M. (2014). A continuous 55-million-year record of transient mantle plume activity beneath Iceland. *Nature Geoscience*, *7*(12), 914–919. https://doi.org/10.1038/ngeo2281

Pease, V., Drachev, S., Stephenson, R., & Zhang, X. (2014). Arctic lithosphere—A review. *Tectonophysics*, *628*, 1–25. https://doi.org/10.1016/j.tecto.2014.05.033

Polteau, S., Hendriks, B. W., Planke, S., Ganerød, M., Corfu, F., Faleide, J. I., et al. (2016). The Early Cretaceous Barents Sea Sill complex: Distribution, $^{40}Ar/^{39}Ar$ geochronology, and implications for carbon gas formation. *Palaeogeography, Palaeoclimatology, Palaeoecology*, *441*, 83–95. https://doi.org/10.1016/j.palaeo.2015.07.007

Rogozhina, I., Petrunin, A. G., Vaughan, A. P. M., Steinberger, B., Johnson, J. V., Kaban, M. K., et al. (2016). Melting at the base of the Greenland ice sheet explained by Iceland hotspot history. *Nature Geoscience*, *9*(5), 366–369. https://doi.org/10.1038/ngeo2689

Saumur, B., Dewing, K., & Williamson, M.-C. (2016). Architecture of the Canadian portion of the high arctic large igneous province and implications for magmatic Ni–Cu potential. *Canadian Journal of Earth Sciences*, *53*(5), 528–542. https://doi.org/10.1139/cjes-2015-0220

Schaeffer, A. J., & Lebedev, S. (2013). Global shear speed structure of the upper mantle and transition zone. *Geophysical Journal International*, *194*(1), 417–449. https://doi.org/10.1093/gji/ggt095

Schmeling, H. (2006). A model of episodic melt extraction for plumes. *Journal of Geophysical Research*, *111*(B3), E003867. https://doi.org/10.1029/2004JB003423

Senger, K., & Galland, O. (2022). Stratigraphic and spatial extent of HALIP magmatism in central Spitsbergen. *Geochemistry, Geophysics, Geosystems*, *23*(11), e2021GC010300. https://doi.org/10.1029/2021GC010300

Shephard, G. E., Müller, R. D., & Seton, M. (2013). The tectonic evolution of the Arctic since Pangea breakup: Integrating constraints from surface geology and geophysics with mantle structure. *Earth-Science Reviews*, *124*, 148–183. https://doi.org/10.1016/j.earscirev.2013.05.012

Shephard, G. E., Trønnes, R. G., Spakman, W., Panet, I., & Gaina, C. (2016). Evidence for slab material under Greenland and links to cretaceous high arctic magmatism. *Geophysical Research Letters*, *43*(8), 3717–3726. https://doi.org/10.1002/2016GL068424

Steffen, R., Audet, P., & Lund, B. (2018). Weakened lithosphere beneath Greenland inferred from effective elastic thickness: A hot spot effect? *Geophysical Research Letters*, *45*(10), 4733–4742. https://doi.org/10.1029/2017GL076885

Steinberger, B., Bredow, E., Lebedev, S., Schaeffer, A., & Torsvik, T. H. (2019). Widespread volcanism in the Greenland–North Atlantic region explained by the Iceland plume. *Nature Geoscience*, *12*(1), 61–68. https://doi.org/10.1038/s41561-018-0251-0

Sun, P., Niu, Y., Guo, P., Duan, M., Wang, X., Gong, H., & Xiao, Y. (2020). The lithospheric thickness control on the compositional variation of continental intraplate basalts: A demonstration using the Cenozoic basalts and Clinopyroxene megacrysts from eastern China. *Journal of Geophysical Research: Solid Earth*, *125*(3), e2019JB019315. https://doi.org/10.1029/2019JB019315

Tarduno, J. (1998). The high arctic large igneous province. In *Third International conference on arctic margins [ICAM III], Celle, Germany, Federal Institute Geoscience Natural Resources Abstract*.

Tegner, C., Storey, M., Holm, P., Thorarinsson, S., Zhao, X., Lo, C.-H., & Knudsen, M. (2011). Magmatism and Eurekan deformation in the high arctic large igneous province: ^{40}Ar–^{39}Ar age of Kap Washington group volcanics, north Greenland. *Earth and Planetary Science Letters*, *303*(3), 203–214. https://doi.org/10.1016/j.epsl.2010.12.047

Thorarinsson, S. B., Holm, P. M., Tappe, S., Heaman, L. M., & Tegner, C. (2011). Late Cretaceous–Palaeocene continental rifting in the high arctic: U–Pb geochronology of the kap Washington group volcanic sequence, north Greenland. *Journal of the Geological Society*, *168*(5), 1093–1106. https://doi.org/10.1144/0016-76492011-018

Trettin, H. (1991). *Geology of Canada, no. 3; geology of the Innuitian orogen and arctic platform of Canada and Greenland* (p. 569). Geological Survey of Canada.

Villeneuve, M., & Williamson, M.-C. (2006). ^{40}Ar-^{39}Ar dating of mafic magmatism from the Sverdrup basin magmatic province. In R. A. Scott & D. K. Thurston (Eds.), *ICAM IV Proceedings, Dartmouth, Nova Scotia* (pp. 206–215).

Zhang, T., Dyment, J., & Gao, J. (2019). Age of the Canada basin, Arctic Ocean: Indications from high-resolution magnetic data. *Geophysical Research Letters*, *46*(23), 13712–13721. https://doi.org/10.1029/2019GL085736